ACCSCIENCE PUBLISHING
An International Journal of Optimization and Control: Theories & Applications
ISSN: 2146-0957 eISSN: 2146-5703
Vol.16, No.5, pp.1721-1744 (2026)
https://doi.org/10.36922/IJOCTA026240117
IJOCTA
RESEARCH ARTICLE

Impact of socio-economic and healthcare structure on epidemic dynamics: Mathematical modeling and optimal control

Khaddouj Taifi[1], Yassine Sabbar[2]*, and Necati Özdemir[3]

[1]IPDAC Team, Department of Informatics, FST Errachidia, Moulay Ismail University of Meknes, Boutalamine, Morocco
[2]IMIA Laboratory, T-IDMS, Department of Mathematics, FST Errachidia, Moulay Ismail University of Meknes, Boutalamine, Errachidia, Morocco
[3]Department of Mathematics, Balıkesir University, Cagıs Campus, Balikesir, Turkiye
k.taifi@umi.ac.ma; y.sabbar@umi.ac.ma; nozdemir@balikesir.edu.tr

ARTICLE INFO

Article history:
Received: June 12, 2026
Revised: July 3, 2026
Accepted: July 13, 2026
Published Online: July 27, 2026

Keywords:
Epidemic model
Socio-economic capacity
Healthcare capacity
Basic reproduction number
Sensitivity analysis
Optimal control

ABSTRACT

We propose and analyze a deterministic SEIR-type epidemic model coupled with two dynamic capacity variables representing socio-economic support and healthcare resources. The resource variables reduce transmission and enhance recovery, whereas infection depletes both capacities, and healthcare operations impose an additional socio-economic cost. We establish positivity, boundedness, and global existence of solutions. The disease-free equilibrium is derived from the coupled resource subsystem, and the associated basic reproduction number $\mathcal{R}_0$ is obtained via the next-generation matrix method. The disease-free equilibrium is locally asymptotically stable when $\mathcal{R}_0 < 1$ and unstable when $\mathcal{R}_0 > 1$. For $\mathcal{R}_0 > 1$, the endemic-equilibrium problem is reduced to a scalar equation, yielding the existence of at least one positive endemic equilibrium; a verifiable monotonicity condition that ensures uniqueness is also provided. We formulate an optimal control problem incorporating prevention, treatment, and healthcare-reinforcement controls, prove the existence of an optimal control, and derive the Pontryagin necessary conditions. For the illustrative baseline parameter set, the full endemic Jacobian has eigenvalues with negative real parts, and the numerical experiments illustrate lower exposed and infectious trajectories under the computed three-control solution of the optimality system.

1. Introduction

Mathematical epidemiology has long provided a rigorous framework for understanding the spread, persistence, and control of infectious diseases.[1] Classical compartmental models, especially of SIR- and SEIR-type, have played a central role in clarifying threshold behavior, long-term dynamics, and the impact of intervention strategies.[2] Their analytical tractability and interpretability have made them fundamental tools in both theoretical epidemiology and public-health decision making.[3] However, despite their success, many standard epidemic models describe disease transmission in a biologically closed manner, without explicitly incorporating the socio-economic and institutional environment within which epidemics evolve.[4,5]

Such a simplification is often restrictive. In practice, epidemic dynamics are strongly influenced by the level of social support, the resilience of healthcare systems, and the broader institutional capacity to absorb and respond to rising disease burden.[6] Weak socio-economic conditions may amplify transmission through increased exposure, reduced prevention, and delayed access

*Corresponding Author

to care, while strong healthcare capacity can mitigate spread, improve recovery, and reduce the persistence of infection.[7] At the same time, epidemics themselves exert substantial pressure on these same support structures by exhausting resources, overloading healthcare facilities, and weakening the surrounding social environment.[8] This reciprocal interaction is essential for understanding not only whether an outbreak occurs, but also why certain epidemics become prolonged, why some systems collapse under sustained pressure, and why control efforts may succeed in one setting but fail in another.[9,10]

These observations motivate epidemic models in which transmission is dynamically coupled with socio-economic and healthcare resources.[11] Relative to biologically closed compartmental systems, this formulation contains two explicit mechanisms:[12] the current resource levels modify transmission and removal,[13] and the epidemic burden modifies the resource levels required for response.[14] The resulting bidirectional coupling introduces an endogenous feedback mechanism for sustained transmission and institutional degradation.[15]

In this paper, we propose and analyze a deterministic six-dimensional SEIR-type model[16] in which the epidemiological compartments S, E, I, R are coupled with two additional variables: a socio-economic support variable Y and a healthcare-resource variable H. The force of infection is reduced through the resource-dependent incidence denominator

$$(1 + aY)(1 + bH)(1 + cI),$$

which accounts simultaneously for the mitigating effects of socio-economic support, healthcare capacity, and saturation in the infectious class. In addition, the removal of infectious individuals depends on the nonlinear recovery function

$$\Gamma(Y, H) = \gamma_0 + \frac{\gamma_1 Y}{m + Y} + \frac{\gamma_2 H}{n + H},$$

so that improvements in support and healthcare resources enhance effective recovery. Conversely, infection pressure depletes both capacities, while maintaining healthcare capacity imposes the socio-economic operating cost represented by $q_2 HY$. These mechanisms create a closed feedback loop between disease prevalence and institutional fragility.

The model leads to four analytical questions: biological well-posedness; identification of the disease-free equilibrium and the invasion threshold; existence and possible uniqueness of positive endemic equilibria; and optimal allocation of prevention, treatment, and healthcare reinforcement when epidemiological and implementation costs are considered.[17]

Recent deterministic epidemic studies emphasize threshold quantities, equilibrium analysis, and intervention assessment in COVID-19 and SVIR models.[18,19] Fractional epidemic formulations and data-based optimal-control studies broaden this perspective by incorporating nonlocal operators or calibrated intervention scenarios.[20,21] Extended SEIR and tuberculosis models further illustrate threshold and stability analysis in structured epidemic systems.[22,23] In the wider theory of differential control systems, existence, continuous dependence, and optimal-control results have also been established for stochastic Hilfer systems with delay, Caputo fractional delay inclusions, and Sobolev-type mixed Volterra-Fredholm equations.[24–26] Stochastic reaction-diffusion epidemic models further account for spatial heterogeneity, population diffusion, and environmental perturbations.[27,28] These contributions provide important analytical frameworks, but they address fractional, stochastic, delayed, spatial, or externally controlled dynamics. The present work instead studies a finite-dimensional deterministic ODE system in which socio-economic support and healthcare capacity are endogenous states that simultaneously reduce incidence, enhance recovery, and deteriorate under system pressure.

Compared with the cited epidemic models, the specific contribution is the closed Y-H feedback architecture: Y and H are not fixed coefficients or prescribed control profiles; they evolve jointly with the SEIR compartments, enter both transmission and recovery, and are depleted through infection and healthcare-operation terms. The control problem then acts on this endogenous resource-coupled system rather than on a biologically isolated SEIR model.

The contributions are fourfold. First, we prove positivity, boundedness, and global existence for the resource-coupled epidemic system. Second, we derive the disease-free equilibrium from the coupled (Y, H) algebraic subsystem, obtain $\mathcal{R}_0$, and prove local stability for $\mathcal{R}_0 < 1$ and instability for $\mathcal{R}_0 > 1$. Third, we reduce the endemic-equilibrium equations to a scalar equation, prove existence for $\mathcal{R}_0 > 1$, and state a sufficient monotonicity condition for uniqueness. The full endemic Jacobian is provided and evaluated for the baseline parameter set. Fourth, we formulate the three-control problem, establish existence of an optimal control, derive the Pontryagin system, and compare the controlled and uncontrolled trajectories numerically.

The novelty is the structural coupling through which socio-economic and healthcare capacities simultaneously enter the incidence and recovery functions while evolving under infection pressure and healthcare-operation costs. Thus, persistent infection can reduce institutional capacity, and reduced capacity can increase effective transmission and weaken recovery. Unlike SEIR-type formulations in which resource effects are fixed coefficients or external inputs, the variables Y and H are endogenous components of the state system.

The numerical study illustrates the threshold dynamics, computes the endemic state, evaluates the full endemic Jacobian, and compares the computed controlled and uncontrolled trajectories. It also reports normalized forward sensitivity indices for the epidemiological and resource parameters. Because the baseline values are synthetic and are not calibrated to a specific outbreak, the numerical results are interpreted as structural demonstrations of the model rather than quantitative forecasts.

The remainder of the paper is organized as follows. In Section 2, we formulate the model and state the standing assumptions on the parameters. Section 3 is devoted to the deterministic analysis, including well-posedness, the disease-free equilibrium, the reproduction number, and endemic equilibria. In Section 4, we formulate the optimal control problem, prove the existence of an optimal control, and derive the Pontryagin maximum principle. Section 5 provides the sensitivity analysis. Section 6 presents numerical experiments illustrating the threshold behavior, endemic dynamics, controlled trajectories, and parameter sensitivity. The paper concludes with a discussion of the main implications and possible extensions of the model.

2. Epidemic-economic model formulation

We formulate a coupled epidemic-economic system in which disease propagation interacts dynamically with two time-dependent support variables: socio-economic support and healthcare capacity. The epidemiological core follows an SEIR-type structure, while the auxiliary variables Y and H encode the available societal and medical resources that influence transmission and recovery. In turn, the epidemic exerts pressure on these same resources, creating a bidirectional feedback loop. The full interaction structure is illustrated in **Figure 1**.

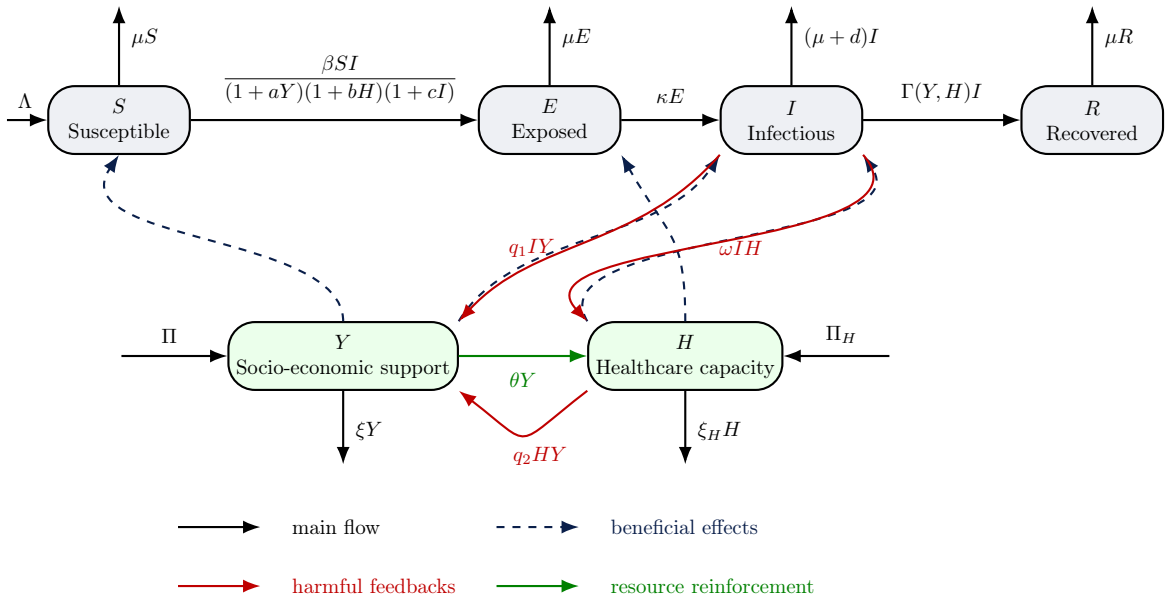

Figure 1. A layered schematic of system (1). The upper layer represents the epidemic progression $S \to E \to I \to R$, while the lower layer contains the socio-economic support variable Y and the healthcare-capacity variable H. Dashed blue arrows represent beneficial resource effects; red arrows represent infection-induced depletion $q_1 IY$, ωIH, and the healthcare operating cost $q_2 HY$; and the green arrow represents reinforcement from socio-economic support to healthcare capacity.

For $t \geq 0$, we consider the six state variables $\big(S(t), E(t), I(t), R(t), Y(t), H(t)\big) \in \mathbb{R}^6_+$, where $S(t)$, $E(t)$, $I(t)$, and $R(t)$ denote susceptible, exposed, infectious, and recovered populations. The variables $Y(t)$ and $H(t)$ are scaled nonnegative effective-capacity indices, not population

compartments and not proportions restricted to $[0, 1]$. Their numerical scales are determined by the replenishment, decay, coupling, and depletion parameters. The index $Y(t)$ aggregates socio-economic resilience, including income stability, access to basic services, compliance capacity, and social support. The index $H(t)$ aggregates effective healthcare capacity, including hospital availability, personnel, diagnostic access, treatment resources, and institutional response strength. The term q_1IY represents infection-induced socio-economic degradation, whereas q_2HY represents the socio-economic operating cost associated with maintaining healthcare capacity; consequently, this term remains active when $I = 0$ and $H > 0$. The term ωIH represents infection-induced depletion of healthcare capacity, while θY represents reinforcement of healthcare capacity by socio-economic support.

The model is governed by the system

$$\begin{cases} \dfrac{\mathrm{d}S}{\mathrm{d}t} = \Lambda - \dfrac{\beta SI}{(1+aY)(1+bH)(1+cI)} - \mu S, \\ \dfrac{\mathrm{d}E}{\mathrm{d}t} = \dfrac{\beta SI}{(1+aY)(1+bH)(1+cI)} - (\mu+\kappa)E, \\ \dfrac{\mathrm{d}I}{\mathrm{d}t} = \kappa E - \left(\mu + d + \gamma_0 + \dfrac{\gamma_1 Y}{m+Y} + \dfrac{\gamma_2 H}{n+H}\right) I, \\ \dfrac{\mathrm{d}R}{\mathrm{d}t} = \left(\gamma_0 + \dfrac{\gamma_1 Y}{m+Y} + \dfrac{\gamma_2 H}{n+H}\right) I - \mu R, \\ \dfrac{\mathrm{d}Y}{\mathrm{d}t} = \Pi - \xi Y - q_1 IY - q_2 HY, \\ \dfrac{\mathrm{d}H}{\mathrm{d}t} = \Pi_H - \xi_H H + \theta Y - \omega IH. \end{cases} \tag{1}$$

The incidence term is defined by $\frac{\beta SI}{(1+aY)(1+bH)(1+cI)}$. This expression combines three distinct effects. The bilinear factor SI models the usual contact-driven generation of new exposed individuals. The factors $(1 + aY)^{-1}$ and $(1 + bH)^{-1}$ quantify the mitigating influence of socio-economic support and healthcare capacity on effective transmission. The factor $(1 + cI)^{-1}$ introduces a nonlinear saturation mechanism, thereby preventing the incidence from growing proportionally to I when prevalence becomes large.

The recovery process is described through the effective treatment-recovery function $\gamma_0 + \frac{\gamma_1 Y}{m+Y} + \frac{\gamma_2 H}{n+H}$, which is increasing and bounded in both Y and H. Thus, stronger socio-economic support and stronger healthcare capacity improve recovery, but with diminishing marginal returns, as reflected by the half-saturation constants m and n.

The resource equations encode the feedback from the epidemic onto the surrounding support systems. The socio-economic variable Y is replenished at rate Π, decays naturally at rate ξ, and is additionally depleted by infection prevalence through q_1IY and by the socio-economic operating cost of healthcare capacity, q_2HY. The healthcare variable H receives exogenous replenishment at rate Π_H, deteriorates naturally at rate ξ_H, is reinforced by socio-economic support through the transfer term θY, and is weakened by infection pressure through the term ωIH. Consequently, system (1) captures a two-way interaction: resources act on epidemic transmission and recovery, while the epidemic simultaneously erodes the resources required for its own control.

For convenience, the model parameters are summarized in **Table 1**.

Throughout the paper we impose the following standing assumptions.

Assumption 1. *All parameters in system* (1) *are nonnegative. In addition, we assume* $\Lambda > 0$, $\mu > 0$, $\beta > 0$, $\kappa > 0$, $\Pi > 0$, $\xi > 0$, $\Pi_H > 0$, $\xi_H > 0$, $m > 0$, $n > 0$, *and at least one of* $\gamma_0, \gamma_1, \gamma_2$ *is strictly positive.*

Assumption 1 guarantees that all nonlinear terms appearing in (1) are well defined on $\mathbb{R}^6_+$. In particular, the denominators $m + Y$, $n + H$, and $(1+aY)(1+bH)(1+cI)$ remain strictly positive for every nonnegative state. Hence the vector field associated with system (1) is of class C^1 on $\mathbb{R}^6_+$. It follows from the classical Cauchy-Lipschitz theorem that, for every nonnegative initial condition, there exists a unique local classical solution.

Allowing $\gamma_1 = 0$ includes the limiting case in which socio-economic support produces no additional saturating recovery contribution. Likewise, $\gamma_2 = 0$ represents a setting in which healthcare capacity does not add a separate saturating recovery term. Requiring at least one of $\gamma_0, \gamma_1, \gamma_2$ to be strictly positive excludes the degenerate case with no recovery mechanism.

From the modeling viewpoint, the central feature of (1) lies in the mutual dependence between epidemic severity and societal resilience. A deterioration in socio-economic or medical capacity may amplify transmission and weaken recovery, whereas sustained infection simultaneously exhausts the very resources needed to contain the outbreak. This endogenous feedback is mathematically responsible for the nontrivial threshold structure and stability behavior established in the subsequent sections.

Table 1. Description of the parameters in system (1)

Parameter	Interpretation
Λ	recruitment rate into the susceptible class,
μ	natural removal rate,
β	baseline transmission coefficient,
a	intensity of the mitigating effect of socio-economic support on transmission,
b	intensity of the mitigating effect of healthcare capacity on transmission,
c	saturation coefficient in the incidence function,
κ	progression rate from exposed to infectious individuals,
d	disease-induced removal rate,
γ_0	baseline recovery rate,
γ_1	maximal additional recovery induced by socio-economic support,
γ_2	maximal additional recovery induced by healthcare capacity,
m	half-saturation constant for the economic contribution to recovery,
n	half-saturation constant for the healthcare contribution to recovery,
Π	replenishment rate of socio-economic support,
ξ	natural decay rate of socio-economic support,
q_1	depletion rate of socio-economic support caused by infection pressure,
q_2	socio-economic operating-cost coefficient associated with healthcare capacity,
Π_H	exogenous replenishment rate of healthcare capacity,
ξ_H	natural decay rate of healthcare capacity,
θ	reinforcement rate from socio-economic support to healthcare capacity,
ω	depletion rate of healthcare capacity caused by infection pressure.

3. Deterministic analysis

In this section, we study the qualitative dynamics of system (1). We first establish positivity, boundedness, and global existence of solutions. We then derive the disease-free equilibrium and its threshold stability condition, and finally analyze endemic equilibria through a scalar reduction.

For convenience, define

$$\Phi(S,I,Y,H) := \frac{\beta SI}{(1+aY)(1+bH)(1+cI)}, \qquad \Gamma(Y,H) := \gamma_0 + \frac{\gamma_1 Y}{m+Y} + \frac{\gamma_2 H}{n+H}. \tag{2}$$

Then system (1) can be written as

$$\begin{cases} \dot{S} = \Lambda - \Phi(S,I,Y,H) - \mu S, \\ \dot{E} = \Phi(S,I,Y,H) - (\mu+\kappa)E, \\ \dot{I} = \kappa E - \big(\mu + d + \Gamma(Y,H)\big)I, \\ \dot{R} = \Gamma(Y,H)I - \mu R, \\ \dot{Y} = \Pi - \xi Y - q_1 IY - q_2 HY, \\ \dot{H} = \Pi_H - \xi_H H + \theta Y - \omega IH. \end{cases} \tag{3}$$

Under Assumption 1, the vector field is of class C^1 on $\mathbb{R}^6_+$. Hence, for every nonnegative initial condition, there exists a unique maximal classical solution.

3.1. Positivity, boundedness, and global existence

We begin by showing that the nonnegative orthant is forward invariant and that every trajectory remains bounded for all future times.

Theorem 1. *Assume Assumption 1. Then for every initial condition* $(S(0),E(0),I(0),R(0),Y(0),H(0)) \in \mathbb{R}^6_+$, *system* (1) *admits a unique global solution* $(S(t),E(t),I(t),R(t),Y(t),H(t)) \in \mathbb{R}^6_+$, $t \geq 0$. *Moreover, if* $N(t) := S(t)+E(t)+I(t)+R(t)$, *then*

$$0 \leq N(t) \leq N(0)e^{-\mu t} + \frac{\Lambda}{\mu}\big(1-e^{-\mu t}\big),\ t \geq 0. \tag{4}$$

In addition,

$$\begin{aligned} 0 \leq Y(t) &\leq Y(0)e^{-\xi t} + \frac{\Pi}{\xi}\big(1-e^{-\xi t}\big) \\ &\leq \max\left\{Y(0), \frac{\Pi}{\xi}\right\}, \end{aligned} \tag{5}$$

and, with

$$M_Y := \max\left\{Y(0), \frac{\Pi}{\xi}\right\},$$

one has

$$0 \leq H(t) \leq H(0)e^{-\xi_H t} + \frac{\Pi_H + \theta M_Y}{\xi_H}\big(1-e^{-\xi_H t}\big). \tag{6}$$

Consequently, every component remains bounded on $[0,\infty)$.

Proof. Since the vector field is locally Lipschitz on $\mathbb{R}^6_+$, there exists a unique maximal solution on some interval $[0,T_{\max})$. We first prove positivity.

Suppose that at some time $t_0 \in [0,T_{\max})$, one component reaches zero while all components remain nonnegative up to time t_0. Then:

$$\dot{S}(t_0) = \Lambda > 0 \text{ whenever } S(t_0) = 0,$$
$$\dot{E}(t_0) = \Phi(S(t_0), I(t_0), Y(t_0), H(t_0)) \geq 0 \text{ whenever } E(t_0) = 0,$$
$$\dot{I}(t_0) = \kappa E(t_0) \geq 0 \text{ whenever } I(t_0) = 0,$$
$$\dot{R}(t_0) = \Gamma(Y(t_0), H(t_0)) I(t_0) \geq 0 \text{ whenever } R(t_0) = 0,$$
$$\dot{Y}(t_0) = \Pi > 0 \text{ whenever } Y(t_0) = 0,$$

and

$$\dot{H}(t_0) = \Pi_H + \theta Y(t_0) \geq 0 \text{ whenever } H(t_0) = 0.$$

Thus, on each boundary hyperplane of $\mathbb{R}^6_+$, the vector field is inward pointing or tangent. By the uniqueness of solutions, no trajectory can cross from $\mathbb{R}^6_+$ to its complement. Therefore $\mathbb{R}^6_+$ is positively invariant.

We now derive the bounds. Summing the first four equations of (3) gives $\dot{N} \leq \Lambda - \mu N$. Comparison with the scalar equation $z' = \Lambda - \mu z,\ z(0) = N(0)$, yields (4). In particular,

$$0 \leq S(t), E(t), I(t), R(t) \leq N(t) \leq M_N,$$

$$M_N := \max\left\{N(0), \frac{\Lambda}{\mu}\right\}.$$

Next,

$$\dot{Y} = \Pi - \xi Y - q_1 I Y - q_2 H Y \leq \Pi - \xi Y.$$

Comparison with

$$z' = \Pi - \xi z,\ z(0) = Y(0),$$

gives (5). Hence

$$0 \leq Y(t) \leq M_Y := \max\left\{Y(0), \frac{\Pi}{\xi}\right\} \text{ for all } t \geq 0.$$

Using this estimate in the H-equation,

$$\dot{H} = \Pi_H - \xi_H H + \theta Y - \omega I H \leq \Pi_H + \theta M_Y - \xi_H H.$$

Comparison with

$$z' = \Pi_H + \theta M_Y - \xi_H z,\ z(0) = H(0),$$

yields (6). Therefore $H(t)$ is also bounded on $[0,\infty)$.

We have shown that all six components remain bounded on every bounded time interval. Since the vector field is locally Lipschitz, boundedness excludes finite-time blow-up. Hence $T_{\max} = \infty$, and the solution is global. □

As an immediate consequence, every trajectory remains in the positively invariant set

$$\Omega_{X_0} := \{(S,E,I,R,Y,H) \in \mathbb{R}^6_+ : S + E + I + R \leq M_N,\ 0 \leq Y \leq M_Y,\ 0 \leq H \leq M_H\},$$

where

$$M_N = \max\left\{N(0), \frac{\Lambda}{\mu}\right\},\ M_Y = \max\left\{Y(0), \frac{\Pi}{\xi}\right\},$$
$$M_H = \max\left\{H(0), \frac{\Pi_H + \theta M_Y}{\xi_H}\right\}.$$

3.2. Disease-free equilibrium and threshold stability

We next derive the disease-free equilibrium and establish its local stability in terms of the basic reproduction number.

Proposition 1. *System* (1) *admits the disease-free equilibrium*

$$E_0 = (S_0, 0, 0, 0, Y_0, H_0), \qquad S_0 = \frac{\Lambda}{\mu}, \tag{7}$$

where $(Y_0, H_0) \in (0,\infty)^2$ *is the unique solution of*

$$\Pi - \xi Y_0 - q_2 H_0 Y_0 = 0, \Pi_H - \xi_H H_0 + \theta Y_0 = 0. \tag{8}$$

Let $B_0 := \xi\xi_H + q_2\Pi_H$. *If* $q_2\theta > 0$, *then*

$$Y_0 = \frac{\sqrt{B_0^2 + 4q_2\theta\Pi\xi_H} - B_0}{2q_2\theta}, H_0 = \frac{\Pi_H + \theta Y_0}{\xi_H}. \tag{9}$$

If $q_2\theta = 0$, *then*

$$Y_0 = \frac{\Pi\xi_H}{\xi\xi_H + q_2\Pi_H}, H_0 = \frac{\Pi_H + \theta Y_0}{\xi_H}. \tag{10}$$

In particular, $Y_0 = \Pi/\xi$ *is recovered when* $q_2 = 0$.

Proof. At the disease-free equilibrium, $E = I = R = 0$. The first equation gives $S_0 = \Lambda/\mu$, while the resource equations are exactly (8). From the second resource equation,

$$H_0 = \frac{\Pi_H + \theta Y_0}{\xi_H}.$$

Substitution into the first resource equation yields

$$q_2\theta Y_0^2 + (\xi\xi_H + q_2\Pi_H) Y_0 - \Pi\xi_H = 0.$$

When $q_2\theta > 0$, the constant term is negative and the quadratic has exactly one positive root, given by (9). When $q_2\theta = 0$, the equation is linear and gives (10). The corresponding H_0 is strictly positive and unique. □

For later use, define

$$S_0 := \frac{\Lambda}{\mu}, \qquad (Y_0, H_0) \text{ by (8)}, \tag{11}$$

and

$$\widehat{\Gamma}_0 := \Gamma(Y_0, H_0) = \gamma_0 + \frac{\gamma_1 Y_0}{m + Y_0} + \frac{\gamma_2 H_0}{n + H_0}, \quad (12)$$
$$\Gamma_0 := \mu + d + \widehat{\Gamma}_0.$$

Proposition 2. *The basic reproduction number of system* (1)*, evaluated at the corrected disease-free resource levels* (Y_0, H_0)*, is*

$$\mathcal{R}_0 = \frac{\beta S_0 \kappa}{(1 + aY_0)(1 + bH_0)(\mu + \kappa)\Gamma_0}. \quad (13)$$

Proof. We use the infected variables (E, I). At the disease-free equilibrium, the new-infection terms and transition terms are

$$\mathcal{F}(E, I) = \begin{pmatrix} \dfrac{\beta S I}{(1 + aY)(1 + bH)(1 + cI)} \\ 0 \end{pmatrix},$$

$$\mathcal{V}(E, I) = \begin{pmatrix} (\mu + \kappa)E \\ -\kappa E + \Gamma_0 I \end{pmatrix}.$$

Therefore,

$$F = \begin{pmatrix} 0 & \dfrac{\beta S_0}{(1 + aY_0)(1 + bH_0)} \\ 0 & 0 \end{pmatrix},$$

$$V = \begin{pmatrix} \mu + \kappa & 0 \\ -\kappa & \Gamma_0 \end{pmatrix}.$$

A direct computation gives

$$V^{-1} = \frac{1}{(\mu + \kappa)\Gamma_0} \begin{pmatrix} \Gamma_0 & 0 \\ \kappa & \mu + \kappa \end{pmatrix}.$$

Hence

$$FV^{-1} = \frac{1}{(\mu + \kappa)\Gamma_0} \begin{pmatrix} \dfrac{\beta S_0 \kappa}{(1 + aY_0)(1 + bH_0)} & \dfrac{\beta S_0 (\mu + \kappa)}{(1 + aY_0)(1 + bH_0)} \\ 0 & 0 \end{pmatrix}.$$

Since FV^{-1} is upper triangular, its eigenvalues are its diagonal entries. Therefore

$$\rho(FV^{-1}) = \frac{\beta S_0 \kappa}{(1 + aY_0)(1 + bH_0)(\mu + \kappa)\Gamma_0},$$

which proves (13). □

We now analyze the local stability of the disease-free equilibrium. Since $\Phi(S, 0, Y, H) = 0$, we have

$$\left.\frac{\partial \Phi}{\partial S}\right|_{E_0} = \left.\frac{\partial \Phi}{\partial Y}\right|_{E_0} = \left.\frac{\partial \Phi}{\partial H}\right|_{E_0} = 0,$$

whereas

$$\left.\frac{\partial \Phi}{\partial I}\right|_{E_0} = \frac{\beta S_0}{(1 + aY_0)(1 + bH_0)}.$$

Therefore the linearized infected block in the variables (E, I) is

$$J_{\inf}(E_0) = \begin{pmatrix} -(\mu + \kappa) & \dfrac{\beta S_0}{(1 + aY_0)(1 + bH_0)} \\ \kappa & -\Gamma_0 \end{pmatrix}. \quad (14)$$

Its characteristic polynomial is

$$\begin{aligned} p_{\inf}(\lambda) &= \det\big(\lambda I_2 - J_{\inf}(E_0)\big) \\ &= \lambda^2 + (\mu + \kappa + \Gamma_0)\lambda \\ &\quad + (\mu + \kappa)\Gamma_0(1 - \mathcal{R}_0). \end{aligned} \quad (15)$$

The remaining four eigenvalues of the full Jacobian at E_0 arise from the decoupled directions S, R, and the resource block (Y, H). Indeed, at E_0, the S-equation contributes the eigenvalue $-\mu$, and the R-equation contributes the eigenvalue $-\mu$. Moreover, the (Y, H)-subsystem is linearized by

$$D = \begin{pmatrix} -(\xi + q_2 H_0) & -q_2 Y_0 \\ \theta & -\xi_H \end{pmatrix}. \quad (16)$$

Its trace and determinant are $\mathrm{tr}(D) = -(\xi + q_2 H_0) - \xi_H < 0$, and $\det(D) = \xi_H(\xi + q_2 H_0) + q_2 Y_0 \theta > 0$. Hence, by the Routh–Hurwitz criterion for 2×2 matrices, both eigenvalues of D have negative real parts.

All entries below are evaluated at the resource equilibrium (Y_0, H_0) defined by (8). We can now state and prove the threshold stability result.

Theorem 2 (Local stability of the disease-free equilibrium)**.** *Let E_0 be the disease-free equilibrium given by* (7)*, and let $\mathcal{R}_0$ be defined by* (13)*. Then:*

(1) if $\mathcal{R}_0 < 1$, then E_0 is locally asymptotically stable;
(2) if $\mathcal{R}_0 > 1$, then E_0 is unstable.

Moreover, in the critical case $\mathcal{R}_0 = 1$, the Jacobian at E_0 has a zero eigenvalue, so the linearization is inconclusive.

Proof. We analyze the Jacobian matrix of system (3) at the disease-free equilibrium $E_0 = (S_0, 0, 0, 0, Y_0, H_0)$. In the variable order (S, E, I, R, Y, H), the full Jacobian at E_0 is

$$J(E_0) = \begin{pmatrix} -\mu & 0 & -\dfrac{\beta S_0}{(1 + aY_0)(1 + bH_0)} & 0 & 0 & 0 \\ 0 & -(\mu + \kappa) & \dfrac{\beta S_0}{(1 + aY_0)(1 + bH_0)} & 0 & 0 & 0 \\ 0 & \kappa & -\Gamma_0 & 0 & 0 & 0 \\ 0 & 0 & \Gamma(Y_0, H_0) & -\mu & 0 & 0 \\ 0 & 0 & -q_1 Y_0 & 0 & -(\xi + q_2 H_0) & -q_2 Y_0 \\ 0 & 0 & -\omega H_0 & 0 & \theta & -\xi_H \end{pmatrix}.$$

This matrix is not block triangular in the present ordering. To reveal its spectral structure,

we permute the coordinates and consider the order (E, I, S, Y, H, R). Let P be the associated permutation matrix. Then $\widetilde{J}(E_0) := P\,J(E_0)\,P^{-1}$ has the same eigenvalues as $J(E_0)$, since permutation similarity preserves the spectrum. In the reordered variables (E, I, S, Y, H, R), the matrix becomes

$$\widetilde{J}(E_0) =$$

$$\begin{pmatrix} -(\mu+\kappa) & \dfrac{\beta S_0}{(1+aY_0)(1+bH_0)} & 0 \\ \kappa & -\Gamma_0 & 0 \\ 0 & -\dfrac{\beta S_0}{(1+aY_0)(1+bH_0)} & -\mu \\ 0 & -q_1 Y_0 & 0 \\ 0 & -\omega H_0 & 0 \\ 0 & \Gamma(Y_0, H_0) & 0 \end{pmatrix}$$

$$\begin{pmatrix} 0 & 0 & 0 \\ 0 & 0 & 0 \\ 0 & 0 & 0 \\ -(\xi + q_2 H_0) & -q_2 Y_0 & 0 \\ \theta & -\xi_H & 0 \\ 0 & 0 & -\mu \end{pmatrix}.$$

This matrix is block lower triangular with diagonal blocks

$$J_{\inf}(E_0) = \begin{pmatrix} -(\mu+\kappa) & \dfrac{\beta S_0}{(1+aY_0)(1+bH_0)} \\ \kappa & -\Gamma_0 \end{pmatrix},$$

$$[-\mu],\ D = \begin{pmatrix} -(\xi + q_2 H_0) & -q_2 Y_0 \\ \theta & -\xi_H \end{pmatrix},\ [-\mu].$$

Hence

$$\sigma(J(E_0)) = \sigma(\widetilde{J}(E_0)) = \sigma\big(J_{\inf}(E_0)\big) \cup \{-\mu\} \cup \sigma(D) \cup \{-\mu\}.$$

We first examine the scalar blocks. Clearly, $-\mu < 0$. Next, for the resource block D, we have $\mathrm{tr}(D) = -(\xi + q_2 H_0) - \xi_H < 0$, and $\det(D) = \xi_H(\xi + q_2 H_0) + q_2 Y_0 \theta > 0$. Therefore, by the Routh–Hurwitz criterion for 2×2 matrices, both eigenvalues of D have negative real parts.

It remains to study the infected block $J_{\inf}(E_0)$. Its characteristic polynomial is

$$p_{\inf}(\lambda) = \det\big(\lambda I_2 - J_{\inf}(E_0)\big) = \lambda^2 + (\mu + \kappa + \Gamma_0)\lambda + (\mu+\kappa)\Gamma_0(1 - \mathcal{R}_0). \tag{17}$$

We now distinguish three cases.

Case 1: $\mathcal{R}_0 < 1$**.** Then $(\mu+\kappa)\Gamma_0(1-\mathcal{R}_0) > 0$. Since also $\mu + \kappa + \Gamma_0 > 0$, both coefficients of the quadratic polynomial (17) are strictly positive. Hence, by the Routh–Hurwitz criterion for quadratic polynomials, both roots of $p_{\inf}$ have negative real parts. Since the other four eigenvalues of $J(E_0)$ also have negative real parts, every eigenvalue of $J(E_0)$ lies in the open left half-plane. Therefore E_0 is locally asymptotically stable.

Case 2: $\mathcal{R}_0 > 1$**.** Then $(\mu+\kappa)\Gamma_0(1-\mathcal{R}_0) < 0$. Thus the constant term of $p_{\inf}$ is negative. Since the leading coefficient is positive, the product of the two roots is negative. Therefore one root is positive and the other is negative. In particular, $J_{\inf}(E_0)$ has a positive eigenvalue, and consequently $J(E_0)$ has a positive eigenvalue. Hence E_0 is unstable.

Case 3: $\mathcal{R}_0 = 1$**.** In this case, $p_{\inf}(\lambda) = \lambda\big(\lambda + \mu + \kappa + \Gamma_0\big)$, so 0 is an eigenvalue of $J_{\inf}(E_0)$, and therefore of $J(E_0)$. Thus the Jacobian is non-hyperbolic, and the linearization does not determine the local dynamics.

This completes the proof. □

Remark 1. *The threshold quantity $\mathcal{R}_0$ depends explicitly on the baseline resource levels Y_0 and H_0. An increase in Y_0 or H_0 enlarges the damping factor $(1 + aY_0)(1 + bH_0)$, which decreases the effective transmission contribution. Moreover, $\Gamma(Y, H)$ is nondecreasing in both Y and H, so larger resource levels also increase the effective removal rate Γ_0. Both mechanisms reduce $\mathcal{R}_0$, thereby favoring local stability of the disease-free equilibrium.*

3.3. Endemic equilibria: reduction and existence

We now investigate steady states corresponding to persistent infection.

An endemic equilibrium is a point $E^* = (S^*, E^*, I^*, R^*, Y^*, H^*) \in \mathbb{R}^6_+$ such that $I^* > 0$. At such an equilibrium, the system satisfies

$$\begin{cases} 0 = \Lambda - \dfrac{\beta S^* I^*}{(1+aY^*)(1+bH^*)(1+cI^*)} - \mu S^*, \\ 0 = \dfrac{\beta S^* I^*}{(1+aY^*)(1+bH^*)(1+cI^*)} - (\mu+\kappa)E^*, \\ 0 = \kappa E^* - \big(\mu + d + \Gamma(Y^*, H^*)\big) I^*, \\ 0 = \Gamma(Y^*, H^*) I^* - \mu R^*, \\ 0 = \Pi - \xi Y^* - q_1 I^* Y^* - q_2 H^* Y^*, \\ 0 = \Pi_H - \xi_H H^* + \theta Y^* - \omega I^* H^*. \end{cases} \tag{18}$$

From the third and fourth equations one immediately obtains

$$R^* = \frac{\Gamma(Y^*, H^*)}{\mu} I^*, \qquad E^* = \frac{\mu + d + \Gamma(Y^*, H^*)}{\kappa} I^*. \tag{19}$$

Combining the second and third equations yields

$$S^* = \frac{(1+aY^*)(1+bH^*)(1+cI^*)(\mu+\kappa)\big(\mu+d+\Gamma(Y^*,H^*)\big)}{\beta\kappa}. \tag{20}$$

The last two equations give

$$Y^* = \frac{\Pi}{\xi+q_1I^*+q_2H^*},\ H^* = \frac{\Pi_H+\theta Y^*}{\xi_H+\omega I^*}. \tag{21}$$

The key point is that, for each fixed infectious level $I \geq 0$, the subsystem for (Y,H) admits a unique positive solution.

Lemma 1. *For each fixed $I \geq 0$, the algebraic system*

$$\begin{cases} Y = \dfrac{\Pi}{\xi+q_1I+q_2H}, \\ H = \dfrac{\Pi_H+\theta Y}{\xi_H+\omega I} \end{cases} \tag{22}$$

admits a unique solution $(Y(I),H(I)) \in (0,\infty)^2$. Moreover, $Y(\cdot)$ and $H(\cdot)$ are continuous on $[0,\infty)$.

Proof. Fix $I \geq 0$. Since $\xi_H+\omega I > 0$, the second equation implies $H = \frac{\Pi_H+\theta Y}{\xi_H+\omega I}$. Substituting this into the first equation, gives

$$Y = \frac{\Pi}{\xi+q_1I+q_2\dfrac{\Pi_H+\theta Y}{\xi_H+\omega I}}.$$

After simplification, this becomes

$$A(I)Y^2 + B(I)Y - \Pi = 0, \tag{23}$$

where

$$A(I) := \frac{q_2\theta}{\xi_H+\omega I} \geq 0,$$

$$B(I) := \xi + q_1I + \frac{q_2\Pi_H}{\xi_H+\omega I} > 0.$$

If $A(I)=0$, then (23) reduces to $B(I)Y-\Pi=0$, which has the unique positive solution $Y(I) = \frac{\Pi}{B(I)} > 0$. If $A(I) > 0$, then (23) is a quadratic polynomial with positive leading coefficient and negative constant term. Hence its two roots have opposite signs, so it has exactly one positive root, namely

$$Y(I) = \frac{-B(I)+\sqrt{B(I)^2+4A(I)\Pi}}{2A(I)} > 0.$$

Once $Y(I)$ is obtained, the second equation gives

$$H(I) = \frac{\Pi_H+\theta Y(I)}{\xi_H+\omega I} > 0.$$

Thus, for each $I \geq 0$, there is a unique positive pair $(Y(I),H(I))$.

The continuity of $Y(I)$ follows from the continuity of $A(I)$ and $B(I)$ together with the explicit formulas above. The continuity of $H(I)$ then follows from its defining formula. □

Lemma 1 reduces the endemic-equilibrium problem to a scalar equation. Define

$$\Psi(I) := \frac{\mu+\kappa}{\kappa}\big(\mu+d+\Gamma(Y(I),H(I))\big) \left[I + \frac{\mu(1+aY(I))(1+bH(I))(1+cI)}{\beta}\right] - \Lambda, I \geq 0. \tag{24}$$

Proposition 3. *A number $I^* > 0$ generates an endemic equilibrium of system* (1) *if and only if*

$$\Psi(I^*) = 0. \tag{25}$$

In that case, $Y^* = Y(I^*)$, $H^* = H(I^*)$, and S^*, E^*, R^* are determined uniquely by (19) *and* (20).

Proof. Suppose first that E^* is an endemic equilibrium. Then (Y^*,H^*) satisfies (22) with $I = I^*$. By Lemma 1, $Y^* = Y(I^*)$, $H^* = H(I^*)$. Substitution of (20) into the first equation of (18)gives exactly $\Psi(I^*) = 0$. Conversely, suppose $I^* > 0$ satisfies $\Psi(I^*) = 0$. Set $Y^* = Y(I^*)$, $H^* = H(I^*)$, and define S^*, E^*, R^* by (19) and (20). By construction, all equations in (18) are satisfied, so the resulting sextuple is an endemic equilibrium. □

We can now prove existence when $\mathcal{R}_0 > 1$.

Theorem 3. *If $\mathcal{R}_0 > 1$, then system* (1) *admits at least one endemic equilibrium with strictly positive components.*

Proof. By Lemma 1, the map $I \mapsto \Psi(I)$ is continuous on $[0,\infty)$. At $I = 0$, Lemma 1 gives the unique pair $(Y(0),H(0)) = (Y_0,H_0)$ satisfying (8). Hence

$$\Psi(0) = \frac{\mu+\kappa}{\kappa}\big(\mu+d+\Gamma(Y_0,H_0)\big) \frac{\mu(1+aY_0)(1+bH_0)}{\beta} - \Lambda.$$

Using $\Gamma(Y_0,H_0) = \widehat{\Gamma}_0$, $\Gamma_0 = \mu+d+\widehat{\Gamma}_0$, and the expression for $\mathcal{R}_0$, we obtain $\Psi(0) = \Lambda\left(\frac{1}{\mathcal{R}_0}-1\right)$. Therefore, $\mathcal{R}_0 > 1 \implies \Psi(0) < 0$. On the other hand, for every $I \geq 0$, $Y(I) > 0$, $H(I) > 0$, and therefore $\Gamma(Y(I),H(I)) \geq \gamma_0$, $(1+aY(I))(1+bH(I))(1+cI) \geq 1$. Using these estimates in (24), we obtain

$$\Psi(I) \geq \frac{\mu+\kappa}{\kappa}(\mu+d+\gamma_0)\left(I+\frac{\mu}{\beta}\right) - \Lambda.$$

The right-hand side tends to $+\infty$ as $I \to +\infty$. Hence

$$\Psi(I) \to +\infty \text{ as } I \to +\infty.$$

Since Ψ is continuous, $\Psi(0) < 0$, and $\Psi(I) \to +\infty$, the intermediate value theorem guarantees the existence of at least one $I^* > 0$ such that $\Psi(I^*) = 0$. Proposition 3 then yields an endemic equilibrium with strictly positive components. □

Remark 2. *Theorem 3 establishes existence, but not unconditional uniqueness, when $\mathcal{R}_0 > 1$. The nonlinear dependence of $Y(I)$ and $H(I)$ on the infectious level can prevent a general monotonicity conclusion for Ψ. A sufficient uniqueness condition is stated below, and the local stability of the baseline endemic equilibrium is assessed from the full Jacobian in Section 6.*

For $I \geq 0$, define

$$\mathcal{A}(I) := \mu + d + \Gamma(Y(I), H(I)),$$
$$\mathcal{B}(I) := (1 + aY(I))(1 + bH(I))(1 + cI).$$

Implicit differentiation of (22) gives

$$\begin{aligned} Y'(I) &= \frac{Y(I)\,[q_2\omega H(I) - q_1(\xi_H + \omega I)]}{\Delta(I)}, \\ H'(I) &= -\frac{\omega H(I)(\xi + q_1 I + q_2 H(I)) + \theta q_1 Y(I)}{\Delta(I)}, \end{aligned} \tag{26}$$

where

$$\Delta(I) := (\xi + q_1 I + q_2 H(I))(\xi_H + \omega I) + q_2\theta Y(I) > 0.$$

Consequently,

$$\begin{aligned} \Psi'(I) = \frac{\mu + \kappa}{\kappa} \Bigg\{ \mathcal{A}'(I) \left[I + \frac{\mu}{\beta}\mathcal{B}(I) \right] \\ + \mathcal{A}(I) \left[1 + \frac{\mu}{\beta}\mathcal{B}'(I) \right] \Bigg\}. \end{aligned} \tag{27}$$

Proposition 4 (Sufficient condition for uniqueness)**.** *Assume $\mathcal{R}_0 > 1$. If, for every $I \geq 0$,*

$$\mathcal{A}(I) \left[1 + \frac{\mu}{\beta}\mathcal{B}'(I) \right] > -\mathcal{A}'(I) \left[I + \frac{\mu}{\beta}\mathcal{B}(I) \right], \tag{28}$$

then $\Psi'(I) > 0$ on $[0, \infty)$. Hence $\Psi(I) = 0$ has exactly one positive root and system (1) *has a unique endemic equilibrium.*

Proof. Condition (28) and (27) imply $\Psi'(I) > 0$. Since $\Psi(0) < 0$ for $\mathcal{R}_0 > 1$ and $\Psi(I) \to +\infty$ as $I \to \infty$, strict monotonicity yields exactly one positive zero. □

Jacobian at an endemic equilibrium. Let

$$\Phi_S = \frac{\beta I}{(1 + aY)(1 + bH)(1 + cI)},$$
$$\Phi_I = \frac{\beta S}{(1 + aY)(1 + bH)(1 + cI)^2},$$
$$\Phi_Y = -\frac{a\beta SI}{(1 + aY)^2(1 + bH)(1 + cI)},$$
$$\Phi_H = -\frac{b\beta SI}{(1 + aY)(1 + bH)^2(1 + cI)},$$

and

$$\Gamma_Y = \frac{\gamma_1 m}{(m + Y)^2}, \qquad \Gamma_H = \frac{\gamma_2 n}{(n + H)^2}.$$

The Jacobian at a general state is

$$J = \begin{pmatrix} -\mu - \Phi_S & 0 & -\Phi_I \\ \Phi_S & -(\mu + \kappa) & \Phi_I \\ 0 & \kappa & -(\mu + d + \Gamma) \\ 0 & 0 & \Gamma \\ 0 & 0 & -q_1 Y \\ 0 & 0 & -\omega H \end{pmatrix} \begin{pmatrix} 0 & -\Phi_Y & -\Phi_H \\ 0 & \Phi_Y & \Phi_H \\ 0 & -\Gamma_Y I & -\Gamma_H I \\ -\mu & \Gamma_Y I & \Gamma_H I \\ 0 & -(\xi + q_1 I + q_2 H) & -q_2 Y \\ 0 & \theta & -(\xi_H + \omega I) \end{pmatrix}. \tag{29}$$

Local asymptotic stability of a computed endemic equilibrium follows when all eigenvalues of $J(E^*)$ have negative real parts.

4. Optimal control problem

We now introduce time-dependent intervention policies into system (1). The aim is to reduce the exposed and infectious populations while balancing the implementation costs of prevention, treatment, and healthcare reinforcement.

4.1. Controlled system and admissible controls

Fix a final time $T > 0$. Let $u_1, u_2, u_3 : [0, T] \to [0, 1]$ be measurable control functions, interpreted respectively as: $u_1(t)$: prevention effort reducing effective transmission, $u_2(t)$: treatment effort increasing the removal rate of infective individuals; and $u_3(t)$: healthcare reinforcement increasing the healthcare-resource level. The controlled model is

$$\begin{cases} \dot{S} = \Lambda - (1 - u_1)\dfrac{\beta SI}{(1 + aY)(1 + bH)(1 + cI)} - \mu S, \\ \dot{E} = (1 - u_1)\dfrac{\beta SI}{(1 + aY)(1 + bH)(1 + cI)} - (\mu + \kappa)E, \\ \dot{I} = \kappa E - \left(\mu + d + \gamma_0 + \dfrac{\gamma_1 Y}{m + Y} + \dfrac{\gamma_2 H}{n + H} + \varrho u_2 \right) I, \\ \dot{R} = \left(\gamma_0 + \dfrac{\gamma_1 Y}{m + Y} + \dfrac{\gamma_2 H}{n + H} + \varrho u_2 \right) I - \mu R, \\ \dot{Y} = \Pi - \xi Y - q_1 IY - q_2 HY, \\ \dot{H} = \Pi_H - \xi_H H + \theta Y - \omega IH + \sigma_H u_3, \end{cases} \tag{30}$$

subject to the nonnegative initial condition. For convenience, define $D(Y,H,I) := (1+aY)(1+bH)(1+cI)$. Then (30) may be written compactly as

$$\begin{cases} \dot{S} = \Lambda - (1-u_1)\dfrac{\beta SI}{D(Y,H,I)} - \mu S, \\ \dot{E} = (1-u_1)\dfrac{\beta SI}{D(Y,H,I)} - (\mu+\kappa)E, \\ \dot{I} = \kappa E - (\mu + d + \Gamma(Y,H) + \varrho u_2)I, \\ \dot{R} = (\Gamma(Y,H) + \varrho u_2)I - \mu R, \\ \dot{Y} = \Pi - \xi Y - q_1 IY - q_2 HY, \\ \dot{H} = \Pi_H - \xi_H H + \theta Y - \omega IH + \sigma_H u_3. \end{cases} \tag{31}$$

The admissible control set is

$$\begin{aligned} &\mathcal{U}_{\text{ad}} := \{u = (u_1,u_2,u_3) \in (L^2(0,T))^3 : \\ &0 \le u_i(t) \le 1 \text{ a.e. on } [0,T],\ i = 1,2,3\}. \end{aligned} \tag{32}$$

The set $\mathcal{U}_{\text{ad}}$ is nonempty, closed, bounded, and convex in the reflexive Hilbert space $(L^2(0,T))^3$; hence it is weakly sequentially compact. The pointwise bounds also imply $u_i \in L^\infty(0,T)$ with $\|u_i\|_\infty \le 1$, which is sufficient for the Carathéodory well-posedness argument.

We minimize the cost functional

$$\begin{aligned} J(u_1,u_2,u_3) = \int_0^T [&A_E E(t) + A_I I(t) \\ &+ \frac{B_1}{2}u_1(t)^2 + \frac{B_2}{2}u_2(t)^2 + \frac{B_3}{2}u_3(t)^2\Big]\,\mathrm{d}t. \end{aligned} \tag{33}$$

Throughout this section we assume $A_E, A_I, B_1, B_2, B_3, \varrho, \sigma_H > 0$, in addition to Assumption 1. The optimal control problem is to find $u^* = (u_1^*, u_2^*, u_3^*) \in \mathcal{U}_{\text{ad}}$ such that

$$J(u^*) = \min_{u \in \mathcal{U}_{\text{ad}}} J(u).$$

4.2. Well-posedness of the controlled dynamics

Theorem 4. *For every $u = (u_1,u_2,u_3) \in \mathcal{U}_{\text{ad}}$ and every nonnegative initial condition, system (30) admits a unique global nonnegative solution*

$$(S,E,I,R,Y,H) \in C([0,T];\mathbb{R}^6_+),$$

and all components remain bounded on $[0,T]$.

Proof. For $u \in \mathcal{U}_{\text{ad}}$, the pointwise constraints imply $u \in (L^\infty(0,T))^3$. The right-hand side of (30) is therefore measurable in t, continuous in the state, and locally Lipschitz in the state uniformly on bounded subsets of $\mathbb{R}^6_+$. Hence, by the Carathéodory existence theorem, there exists a unique maximal absolutely continuous solution on some interval $[0, T_{\max}) \subset [0,T]$.

To prove positivity, assume that one component reaches zero at some time while all components remain nonnegative beforehand. Then

$$\dot{S}\big|_{S=0} = \Lambda \ge 0,\ \dot{E}\big|_{E=0} = (1-u_1)\frac{\beta SI}{D(Y,H,I)} \ge 0,$$

$$\dot{I}\big|_{I=0} = \kappa E \ge 0,\ \dot{R}\big|_{R=0} = (\Gamma(Y,H) + \varrho u_2)I \ge 0,$$

$$\dot{Y}\big|_{Y=0} = \Pi \ge 0,\ \dot{H}\big|_{H=0} = \Pi_H + \theta Y + \sigma_H u_3 \ge 0.$$

Thus the nonnegative orthant is positively invariant. Also, we have

$$\begin{aligned} 0 \le N(t) &\le N(0)e^{-\mu t} + \frac{\Lambda}{\mu}(1 - e^{-\mu t}) \\ &\le \max\left\{N(0), \frac{\Lambda}{\mu}\right\}, \end{aligned} \tag{34}$$

and

$$\begin{aligned} 0 \le Y(t) &\le Y(0)e^{-\xi t} + \frac{\Pi}{\xi}(1 - e^{-\xi t}) \\ &\le M_Y := \max\left\{Y(0), \frac{\Pi}{\xi}\right\}. \end{aligned} \tag{35}$$

Finally, since $0 \le u_3 \le 1$ a.e. and $Y(t) \le M_Y$, we have

$$\begin{aligned} 0 \le H(t) &\le H(0)e^{-\xi_H t} \\ &+ \frac{\Pi_H + \theta M_Y + \sigma_H}{\xi_H}(1 - e^{-\xi_H t}). \end{aligned} \tag{36}$$

Thus all state variables remain bounded on $[0, T_{\max})$. Since the vector field is locally Lipschitz in the state and the solution stays bounded, finite-time blow-up cannot occur. Therefore $T_{\max} = T$, and the solution exists uniquely on $[0,T]$. □

4.3. Existence of an optimal control

Theorem 5. *There exists at least one optimal control $u^* = (u_1^*, u_2^*, u_3^*) \in \mathcal{U}_{\text{ad}}$ such that $J(u^*) = \min_{u \in \mathcal{U}_{\text{ad}}} J(u)$.*

Proof. Define $J_* := \inf_{u \in \mathcal{U}_{\text{ad}}} J(u)$. Since the integrand in (33) is nonnegative, $J_* \ge 0$. Let $(u^{(n)})_{n \ge 1} \subset \mathcal{U}_{\text{ad}}$ be a minimizing sequence such that

$$J(u^{(n)}) \longrightarrow J_*.$$

For each n, let $x^{(n)} = (S^{(n)}, E^{(n)}, I^{(n)}, R^{(n)}, Y^{(n)}, H^{(n)})$ be the unique state trajectory associated with $u^{(n)}$. By Theorem 4, all trajectories $x^{(n)}$ remain in a common bounded subset of $\mathbb{R}^6_+$, independent of n. Moreover, from the state equations (31) and these uniform bounds, there exists a constant $C_T > 0$, independent of n, such that $\|\dot{x}^{(n)}\|_{L^\infty(0,T;\mathbb{R}^6)} \le C_T$. Hence the sequence $(x^{(n)})$ is uniformly bounded and equi-Lipschitz on $[0,T]$. By the Arzelà–Ascoli theorem, there exist a subsequence, still denoted $(x^{(n)})$, and a function

$$x^* = (S^*, E^*, I^*, R^*, Y^*, H^*) \in C([0,T];\mathbb{R}^6_+)$$

such that

$$x^{(n)} \to x^* \text{ uniformly on } [0,T].$$

We next consider the controls. Since $0 \le u_i^{(n)}(t) \le 1$ a.e. on $[0,T]$, the sequence $(u^{(n)})$ is bounded in $(L^2(0,T))^3$. Because $(L^2(0,T))^3$ is reflexive, there exist a subsequence, not relabeled, and a function

$$u^* = (u_1^*, u_2^*, u_3^*) \in (L^2(0,T))^3$$

such that

$$u^{(n)} \rightharpoonup u^* \text{ weakly in } (L^2(0,T))^3.$$

Since $\mathcal{U}_{\text{ad}}$ is convex and closed in $(L^2(0,T))^3$, it is weakly closed. Therefore $u^* \in \mathcal{U}_{\text{ad}}$.

We now prove that x^* is the state trajectory corresponding to the control u^*. Write the state system in integral form:

$$x^{(n)}(t) = x_0 + \int_0^t f(x^{(n)}(s), u^{(n)}(s))\,\mathrm{d}s,\ t \in [0,T].$$

We pass to the limit component by component. Set

$$\phi_n(t) := \frac{\beta S^{(n)}(t) I^{(n)}(t)}{D(Y^{(n)}(t), H^{(n)}(t), I^{(n)}(t))},$$

$$\phi^*(t) := \frac{\beta S^*(t) I^*(t)}{D(Y^*(t), H^*(t), I^*(t))}.$$

Since $x^{(n)} \to x^*$ uniformly and the denominator $D(Y,H,I) \ge 1$, we have

$$\phi_n \to \phi^* \text{ uniformly on } [0,T].$$

Let $\psi \in L^2(0,T)$. Then

$$\begin{aligned}\int_0^T \Big((1-u_1^{(n)})\phi_n - (1-u_1^*)\phi^*\Big)\psi\,\mathrm{d}t &= \int_0^T (1-u_1^{(n)})(\phi_n - \phi^*)\psi\,\mathrm{d}t \\ &\quad + \int_0^T (u_1^* - u_1^{(n)})\phi^*\psi\,\mathrm{d}t.\end{aligned}$$

Because $0 \le 1-u_1^{(n)} \le 1$ and $\phi_n \to \phi^*$ uniformly,

$$\begin{aligned}&\left|\int_0^T (1-u_1^{(n)})(\phi_n - \phi^*)\psi\,\mathrm{d}t\right| \\ &\le \|\phi_n - \phi^*\|_{L^\infty}\|\psi\|_{L^1} \longrightarrow 0.\end{aligned}$$

Since $\phi^*\psi \in L^2(0,T)$ and $u_1^{(n)} \rightharpoonup u_1^*$ weakly in $L^2(0,T)$,

$$\int_0^T (u_1^* - u_1^{(n)})\phi^*\psi\,\mathrm{d}t \longrightarrow 0.$$

Thus

$$(1-u_1^{(n)})\phi_n \rightharpoonup (1-u_1^*)\phi^* \text{ weakly in } L^2(0,T).$$

Similarly, since $I^{(n)} \to I^*$ uniformly and $u_2^{(n)} \rightharpoonup u_2^*$ weakly in $L^2(0,T)$, we obtain

$$u_2^{(n)} I^{(n)} \rightharpoonup u_2^* I^* \text{ weakly in } L^2(0,T).$$

Likewise,

$$u_3^{(n)} \rightharpoonup u_3^* \text{ weakly in } L^2(0,T).$$

All remaining terms in the state equations depend only on the state variables, and therefore converge uniformly on $[0,T]$. Passing to the limit in each integral equation, we conclude that x^* satisfies (31) with control u^* and the prescribed initial data. By uniqueness of solutions to the controlled system, x^* is exactly the state trajectory associated with u^*.

It remains to prove optimality. Since $x^{(n)} \to x^*$ uniformly on $[0,T]$,

$$\int_0^T \big(A_E E^{(n)}(t) + A_I I^{(n)}(t)\big)\mathrm{d}t \longrightarrow \int_0^T \big(A_E E^*(t) + A_I I^*(t)\big)\mathrm{d}t.$$

On the other hand, the map

$$u \mapsto \int_0^T \left(\frac{B_1}{2}u_1^2 + \frac{B_2}{2}u_2^2 + \frac{B_3}{2}u_3^2\right)\mathrm{d}t$$

is convex and weakly lower semicontinuous on $(L^2(0,T))^3$. Therefore

$$\int_0^T \frac{B_i}{2}\big(u_i^*(t)\big)^2\,\mathrm{d}t \le \liminf_{n\to\infty} \int_0^T \frac{B_i}{2}\big(u_i^{(n)}(t)\big)^2\,\mathrm{d}t, \quad i = 1,2,3.$$

Combining these facts yields

$$J(u^*) \le \liminf_{n\to\infty} J(u^{(n)}) = J_*.$$

Since $J_* \le J(u^*)$ by definition of the infimum, we conclude that $J(u^*) = J_*$. Hence u^* is an optimal control. □

4.4. Pontryagin maximum principle

Let $x = (S,E,I,R,Y,H)$, and $\lambda = (\lambda_1,\lambda_2,\lambda_3,\lambda_4,\lambda_5,\lambda_6)$ denote the state and adjoint variables. The Hamiltonian associated with (30)–(33) is

$$\begin{aligned}\mathcal{H} &= A_E E + A_I I + \frac{B_1}{2}u_1^2 + \frac{B_2}{2}u_2^2 + \frac{B_3}{2}u_3^2 \\ &\quad + \lambda_1\left(\Lambda - (1-u_1)\frac{\beta SI}{D(Y,H,I)} - \mu S\right) \\ &\quad + \lambda_2\left((1-u_1)\frac{\beta SI}{D(Y,H,I)} - (\mu+\kappa)E\right) \\ &\quad + \lambda_3\left(\kappa E - (\mu + d + \Gamma(Y,H) + \varrho u_2)I\right) \\ &\quad + \lambda_4\left((\Gamma(Y,H) + \varrho u_2)I - \mu R\right) \\ &\quad + \lambda_5\left(\Pi - \xi Y - q_1 IY - q_2 HY\right) \\ &\quad + \lambda_6\left(\Pi_H - \xi_H H + \theta Y - \omega IH + \sigma_H u_3\right).\end{aligned} \tag{37}$$

For convenience, define

$$F(S,I,Y,H;u_1) := (1-u_1)\frac{\beta SI}{D(Y,H,I)}. \tag{38}$$

Its partial derivatives are

$$F_S = (1-u_1)\frac{\beta I}{D(Y,H,I)}, \tag{39}$$

$$F_I = (1-u_1)\frac{\beta S}{(1+aY)(1+bH)(1+cI)^2}, \tag{40}$$

$$F_Y = -(1-u_1)\frac{a\beta SI}{(1+aY)^2(1+bH)(1+cI)}, \tag{41}$$

$$F_H = -(1-u_1)\frac{b\beta SI}{(1+aY)(1+bH)^2(1+cI)}, \tag{42}$$

and

$$\Gamma_Y(Y,H) = \frac{\gamma_1 m}{(m+Y)^2}, \Gamma_H(Y,H) = \frac{\gamma_2 n}{(n+H)^2}. \tag{43}$$

Theorem 6. *Let $u^* = (u_1^*, u_2^*, u_3^*) \in \mathcal{U}_{\text{ad}}$ be an optimal control and let*

$$x^* = (S^*, E^*, I^*, R^*, Y^*, H^*)$$

be the corresponding state trajectory. Then there exist absolutely continuous adjoint functions

$$\lambda_i : [0,T] \to \mathbb{R},\ i = 1, \dots, 6,$$

such that

$$\dot{\lambda}_i(t) = -\frac{\partial \mathcal{H}}{\partial x_i}\big(x^*(t), u^*(t), \lambda(t)\big),\ i = 1, \dots, 6,$$

with transversality conditions

$$\begin{aligned} &\lambda_1(T) = \lambda_2(T) = \lambda_3(T) = \lambda_4(T) \\ &= \lambda_5(T) = \lambda_6(T) = 0. \end{aligned} \tag{44}$$

Equivalently, the adjoint system is

$$\begin{cases} \dot{\lambda}_1 = \mu\lambda_1 + (\lambda_1 - \lambda_2)F_S, \\ \dot{\lambda}_2 = -A_E + (\mu+\kappa)\lambda_2 - \kappa\lambda_3, \\ \dot{\lambda}_3 = -A_I + (\lambda_1 - \lambda_2)F_I \\ \quad + (\mu + d + \Gamma(Y,H) + \varrho u_2)\lambda_3 \\ \quad - (\Gamma(Y,H) + \varrho u_2)\lambda_4 + q_1 Y\lambda_5 + \omega H\lambda_6, \\ \dot{\lambda}_4 = \mu\lambda_4, \\ \dot{\lambda}_5 = (\lambda_1 - \lambda_2)F_Y + (\lambda_3 - \lambda_4)\Gamma_Y(Y,H)\, I \\ \quad + (\xi + q_1 I + q_2 H)\lambda_5 - \theta\lambda_6, \\ \dot{\lambda}_6 = (\lambda_1 - \lambda_2)F_H + (\lambda_3 - \lambda_4)\Gamma_H(Y,H)\, I \\ \quad + q_2 Y\lambda_5 + (\xi_H + \omega I)\lambda_6. \end{cases} \tag{45}$$

Moreover, the optimal controls satisfy, for a.e. $t \in [0,T]$,

$$u_1^*(t) = \Pi_{[0,1]}\left(\frac{(\lambda_2 - \lambda_1)\beta S^* I^*}{B_1 D(Y^*, H^*, I^*)}\right), \tag{46}$$

$$u_2^*(t) = \Pi_{[0,1]}\left(\frac{\varrho I^*(\lambda_3 - \lambda_4)}{B_2}\right), \tag{47}$$

$$u_3^*(t) = \Pi_{[0,1]}\left(-\frac{\sigma_H \lambda_6}{B_3}\right), \tag{48}$$

where $\Pi_{[0,1]}(z) := \min\{1, \max\{0, z\}\}$.

Proof. Since the terminal state is free and the cost functional contains no terminal payoff, the Pontryagin maximum principle yields the transversality condition (44) and the adjoint system

$$\dot{\lambda} = -\nabla_x \mathcal{H}(x^*, u^*, \lambda).$$

The extremal is normal. Indeed, if the cost multiplier were zero, then the adjoint equation would be a homogeneous linear system with terminal condition $\lambda(T) = 0$, and therefore $\lambda \equiv 0$. This would violate the nontriviality condition of the maximum principle. Hence the cost multiplier is normalized to one in the Hamiltonian above.

We compute the state derivatives of the Hamiltonian.

For the variable S,

$$\frac{\partial \mathcal{H}}{\partial S} = \lambda_1(-F_S - \mu) + \lambda_2 F_S,$$

and therefore

$$\dot{\lambda}_1 = -\frac{\partial \mathcal{H}}{\partial S} = \mu\lambda_1 + (\lambda_1 - \lambda_2)F_S.$$

For E,

$$\frac{\partial \mathcal{H}}{\partial E} = A_E - \lambda_2(\mu + \kappa) + \kappa\lambda_3,$$

hence

$$\dot{\lambda}_2 = -\frac{\partial \mathcal{H}}{\partial E} = -A_E + (\mu+\kappa)\lambda_2 - \kappa\lambda_3.$$

For I,

$$\begin{aligned} \frac{\partial \mathcal{H}}{\partial I} &= A_I - \lambda_1 F_I + \lambda_2 F_I - \lambda_3(\mu + d + \Gamma + \varrho u_2) \\ &\quad + \lambda_4(\Gamma + \varrho u_2) - \lambda_5 q_1 Y - \lambda_6 \omega H, \end{aligned}$$

so

$$\begin{aligned} \dot{\lambda}_3 = -\frac{\partial \mathcal{H}}{\partial I} &= -A_I + (\lambda_1 - \lambda_2)F_I + (\mu + d + \Gamma + \varrho u_2)\lambda_3 \\ &\quad - (\Gamma + \varrho u_2)\lambda_4 + q_1 Y\lambda_5 + \omega H\lambda_6. \end{aligned}$$

For R,

$$\frac{\partial \mathcal{H}}{\partial R} = -\mu\lambda_4,\ \dot{\lambda}_4 = \mu\lambda_4.$$

For Y,

$$\begin{aligned} \frac{\partial \mathcal{H}}{\partial Y} &= -\lambda_1 F_Y + \lambda_2 F_Y - \lambda_3 \Gamma_Y I + \lambda_4 \Gamma_Y I \\ &\quad - \lambda_5(\xi + q_1 I + q_2 H) + \theta\lambda_6, \end{aligned}$$

hence

$$\begin{aligned} \dot{\lambda}_5 &= (\lambda_1 - \lambda_2)F_Y + (\lambda_3 - \lambda_4)\Gamma_Y I \\ &\quad + (\xi + q_1 I + q_2 H)\lambda_5 - \theta\lambda_6. \end{aligned}$$

For H,

$$\begin{aligned} \frac{\partial \mathcal{H}}{\partial H} &= -\lambda_1 F_H + \lambda_2 F_H - \lambda_3 \Gamma_H I + \lambda_4 \Gamma_H I \\ &\quad - \lambda_5 q_2 Y - \lambda_6(\xi_H + \omega I), \end{aligned}$$

thus

$$\dot{\lambda}_6 = (\lambda_1 - \lambda_2)F_H + (\lambda_3 - \lambda_4)\Gamma_H I$$

$$+q_2 Y\lambda_5 + (\xi_H + \omega I)\lambda_6.$$

We next characterize the optimal controls. The Hamiltonian is strictly convex with respect to $u = (u_1, u_2, u_3)$, since

$$\frac{\partial^2 \mathcal{H}}{\partial u_1^2} = B_1 > 0,\ \frac{\partial^2 \mathcal{H}}{\partial u_2^2} = B_2 > 0,\ \frac{\partial^2 \mathcal{H}}{\partial u_3^2} = B_3 > 0.$$

Hence the pointwise minimizer is uniquely determined by the first-order stationarity conditions:

$$\frac{\partial \mathcal{H}}{\partial u_1} = B_1 u_1 + \frac{\beta SI}{D(Y,H,I)}(\lambda_1 - \lambda_2) = 0,$$
$$\frac{\partial \mathcal{H}}{\partial u_2} = B_2 u_2 + \varrho I(\lambda_4 - \lambda_3) = 0,$$
$$\frac{\partial \mathcal{H}}{\partial u_3} = B_3 u_3 + \sigma_H \lambda_6 = 0.$$

Therefore the unconstrained minimizers are

$$u_1 = \frac{(\lambda_2 - \lambda_1)\beta SI}{B_1 D(Y,H,I)},\ u_2 = \frac{\varrho I(\lambda_3 - \lambda_4)}{B_2},$$
$$u_3 = -\frac{\sigma_H \lambda_6}{B_3}.$$

Projecting onto the admissible interval $[0,1]$ yields (46)–(48). □

4.5. Optimality system and local uniqueness

The optimality system consists of the state equations (30), the adjoint equations (45), the initial conditions for the state variables, the terminal conditions (44) for the adjoint variables, and the feedback laws (46)−(48). The state system is solved forward in time, whereas the adjoint system is solved backward.

Theorem 7. *There exists $T_0 > 0$ such that, for every $T \in (0, T_0)$, the optimality system admits at most one bounded solution.*

Proof. Let (x, λ, u) and $(\bar{x}, \bar{\lambda}, \bar{u})$ be two bounded solutions of the optimality system on $[0,T]$. Fix an arbitrary $\overline{T} > 0$ and restrict $T \le \overline{T}$. The comparison bounds in Theorem 4 place every admissible state trajectory in a compact set that is independent of the particular control. Moreover, the adjoint system has the form $\dot{\lambda} = A(t)\lambda + b$, where $A(t)$ is uniformly bounded on this state set and $b = (0, -A_E, -A_I, 0, 0, 0)^T$. An application of the backward Gronwall inequality gives

$$\|\lambda\|_{L^\infty(0,T)} \le \|b\| T e^{C_A T} \le \|b\| \overline{T} e^{C_A \overline{T}},$$

and the same estimate holds for $\bar{\lambda}$. Thus the state and adjoint bounds used below are uniform over all solutions with $T \le \overline{T}$. Because

$$D(Y,H,I) \ge 1,\ m + Y \ge m > 0,\ n + H \ge n > 0,$$

all coefficients in the state and adjoint systems are uniformly Lipschitz on this fixed bounded set.

Since the projection operator $\Pi_{[0,1]}$ is 1-Lipschitz, the feedback laws (46)–(48) imply the existence of a constant $C_1 > 0$ such that

$$|u(t) - \bar{u}(t)| \le C_1\big(|x(t) - \bar{x}(t)| + |\lambda(t) - \bar{\lambda}(t)|\big) \quad (49)$$

for almost every $t \in [0,T]$.

Let f denote the right-hand side of the state system. Since f is Lipschitz in (x,u) on the relevant bounded set, there exists $C_2 > 0$ such that

$$|\dot{x}(t) - \dot{\bar{x}}(t)| \le C_2\big(|x(t) - \bar{x}(t)| + |u(t) - \bar{u}(t)|\big).$$

Using (49), we obtain

$$|\dot{x}(t) - \dot{\bar{x}}(t)| \le C_3\big(|x(t) - \bar{x}(t)| + |\lambda(t) - \bar{\lambda}(t)|\big)$$

for some $C_3 > 0$. Since $x(0) = \bar{x}(0)$, integration gives

$$|x(t) - \bar{x}(t)| \le C_3 \int_0^t \big(|x(s) - \bar{x}(s)| + |\lambda(s) - \bar{\lambda}(s)|\big)\mathrm{d}s. \quad (50)$$

Similarly, let g denote the right-hand side of the adjoint system. Since g is Lipschitz in (x, λ, u) on bounded sets, there exists $C_4 > 0$ such that

$$|\dot{\lambda}(t) - \dot{\bar{\lambda}}(t)| \le C_4\big(|x(t) - \bar{x}(t)| + |\lambda(t) - \bar{\lambda}(t)| + |u(t) - \bar{u}(t)|\big).$$

Again using (49), we infer

$$|\dot{\lambda}(t) - \dot{\bar{\lambda}}(t)| \le C_5\big(|x(t) - \bar{x}(t)| + |\lambda(t) - \bar{\lambda}(t)|\big)$$

for some $C_5 > 0$. Since $\lambda(T) = \bar{\lambda}(T) = 0$, backward integration yields

$$|\lambda(t) - \bar{\lambda}(t)| \le C_5 \int_t^T \big(|x(s) - \bar{x}(s)| + |\lambda(s) - \bar{\lambda}(s)|\big)\mathrm{d}s. \quad (51)$$

Define

$$M := \sup_{0 \le t \le T} |x(t) - \bar{x}(t)| + \sup_{0 \le t \le T} |\lambda(t) - \bar{\lambda}(t)|.$$

Taking the supremum in (50) and (51), we obtain

$$\sup_{0 \le t \le T} |x(t) - \bar{x}(t)| \le C_3 T M,$$
$$\sup_{0 \le t \le T} |\lambda(t) - \bar{\lambda}(t)| \le C_5 T M.$$

Hence

$$M \le (C_3 + C_5) T M.$$

Choose $T_0 > 0$ such that

$$(C_3 + C_5) T_0 < 1.$$

Then, for every $T \in (0, T_0)$, the above inequality implies $M = 0$. Therefore

$$x = \bar{x},\ \lambda = \bar{\lambda},$$

and then (49) yields $u = \bar{u}$ almost everywhere on $[0,T]$. This proves uniqueness. □

Remark 3. *The short-time uniqueness obtained in Theorem 7 is standard for nonlinear forward-backward optimality systems. Global uniqueness on arbitrary horizons generally requires additional monotonicity or smallness conditions.*

5. Sensitivity analysis of the basic reproduction number

For a parameter p, the normalized forward sensitivity index is

$$\Upsilon_p^{\mathcal{R}_0} := \frac{\partial \mathcal{R}_0}{\partial p}\frac{p}{\mathcal{R}_0}. \tag{52}$$

A positive value indicates that a relative increase in p increases $\mathcal{R}_0$, whereas a negative value indicates a decrease.

The direct contributions are

$$\Upsilon_\beta^{\mathcal{R}_0} = 1, \Upsilon_\Lambda^{\mathcal{R}_0} = 1, \Upsilon_\kappa^{\mathcal{R}_0} = \frac{\mu}{\mu+\kappa}, \Upsilon_c^{\mathcal{R}_0} = 0, \tag{53}$$

$$\Upsilon_\mu^{\mathcal{R}_0} = -1 - \frac{\mu}{\mu+\kappa} - \frac{\mu}{\Gamma_0}, \Upsilon_d^{\mathcal{R}_0} = -\frac{d}{\Gamma_0},$$

$$\Upsilon_{\gamma_0}^{\mathcal{R}_0} = -\frac{\gamma_0}{\Gamma_0}, \tag{54}$$

$$\Upsilon_{\gamma_1}^{\mathcal{R}_0} = -\frac{\gamma_1 Y_0}{\Gamma_0(m+Y_0)},$$

$$\Upsilon_{\gamma_2}^{\mathcal{R}_0} = -\frac{\gamma_2 H_0}{\Gamma_0(n+H_0)}, \tag{55}$$

$$\Upsilon_m^{\mathcal{R}_0} = \frac{m\gamma_1 Y_0}{\Gamma_0(m+Y_0)^2}, \Upsilon_n^{\mathcal{R}_0} = \frac{n\gamma_2 H_0}{\Gamma_0(n+H_0)^2}, \tag{56}$$

$$\Upsilon_a^{\mathcal{R}_0} = -\frac{aY_0}{1+aY_0}, \Upsilon_b^{\mathcal{R}_0} = -\frac{bH_0}{1+bH_0}. \tag{57}$$

The zero index for c follows because the threshold is evaluated at $I = 0$.

The parameters $\Pi, \xi, q_2, \Pi_H, \xi_H, \theta$ act through the coupled resource equilibrium. Define

$$M_0 := \begin{pmatrix} \xi + q_2 H_0 & q_2 Y_0 \\ -\theta & \xi_H \end{pmatrix},$$

which is nonsingular because

$$\det M_0 = \xi_H(\xi + q_2 H_0) + q_2\theta Y_0 > 0.$$

For $p \in \{\Pi, \xi, q_2, \Pi_H, \xi_H, \theta\}$, the derivatives of the resource equilibrium satisfy

$$M_0 \begin{pmatrix} \partial_p Y_0 \\ \partial_p H_0 \end{pmatrix} = r_p, \tag{58}$$

where

$$r_\Pi = \begin{pmatrix} 1 \\ 0 \end{pmatrix}, \quad r_\xi = \begin{pmatrix} -Y_0 \\ 0 \end{pmatrix}, \quad r_{q_2} = \begin{pmatrix} -H_0 Y_0 \\ 0 \end{pmatrix},$$

$$r_{\Pi_H} = \begin{pmatrix} 0 \\ 1 \end{pmatrix}, \quad r_{\xi_H} = \begin{pmatrix} 0 \\ -H_0 \end{pmatrix}, \quad r_\theta = \begin{pmatrix} 0 \\ Y_0 \end{pmatrix}.$$

Let

$$C_Y := \frac{a}{1+aY_0} + \frac{\gamma_1 m}{\Gamma_0(m+Y_0)^2},$$

$$C_H := \frac{b}{1+bH_0} + \frac{\gamma_2 n}{\Gamma_0(n+H_0)^2}.$$

Then

$$\Upsilon_p^{\mathcal{R}_0} = -p\left(C_Y \partial_p Y_0 + C_H \partial_p H_0\right), \quad p \in \{\Pi, \xi, q_2, \Pi_H, \xi_H, \theta\}. \tag{59}$$

Moreover, $\Upsilon_{q_1}^{\mathcal{R}_0} = \Upsilon_\omega^{\mathcal{R}_0} = 0$, because the corresponding terms contain I and vanish at the disease-free equilibrium.

For the baseline parameter set in **Table 2**,the corrected resource equilibrium is

$$Y_0 = 19.92022364, H_0 = 114.00079872,$$

$$R_0 = 7.12443853.$$

The numerical indices are reported in **Table 3**. The largest positive indices correspond to β and Λ, both equal to one. The most negative index is associated with μ, followed by b, Π, and γ_2. For this parameter set, increasing q_2, ξ, or ξ_H increases $\mathcal{R}_0$, whereas increasing Π, Π_H, or θ decreases $\mathcal{R}_0$. These signs are consequences specific to the baseline coupled disease-free resource equations and are not asserted as universal parameter monotonicities. To better illustrate the numerical behavior of the different indices, we present the results in **Figure 2**.

6. Numerical investigations and model-based interpretation

This section illustrates the threshold dynamics, computes and verifies a positive endemic equilibrium, evaluates the Jacobian spectra at the disease-free and endemic equilibria, and compares uncontrolled and controlled trajectories. The parameter set is a synthetic benchmark and was not fitted to a specific epidemic data set. Accordingly, the numerical results illustrate the internal behavior of the proposed model and should not be interpreted as epidemiological forecasts or direct policy estimates.

All computations and figures were produced in MATLAB. The uncontrolled trajectories and the one-parameter simulations were integrated with `ode45`, with relative and absolute tolerances 10^{-9} and 10^{-10}, respectively. For the optimality system, the interval $[0, 120]$ was divided into $N = 1200$ subintervals, giving the fixed step size $h = 0.1$. The state and adjoint equations were integrated by the classical fourth-order Runge-Kutta method within a forward-backward sweep algorithm. The controls were initialized as

$$u_1^{(0)}(t) = u_2^{(0)}(t) = u_3^{(0)}(t) = 0,$$

and updated according to

$$u^{(k+1)} = 0.98u^{(k)} + 0.02\widehat{u}^{(k)},$$

where $\widehat{u}^{(k)}$ denotes the projected controls obtained from (46)–(48). The stopping criterion was

$$\max_{1\le j\le 3}\left\|u_j^{(k+1)}-u_j^{(k)}\right\|_\infty < 10^{-8},$$

with a maximum number of 12000 iterations. The algorithm converged after 6252 iterations. The discrete objective functional was evaluated with the composite trapezoidal rule using MATLAB's `trapz` function.

6.1. Numerical simulations

The initial state is

$$(S(0),E(0),I(0),R(0),Y(0),H(0)) = (3500,40,25,10,35,20).$$

Table 3 lists the baseline parameter values used throughout the simulations.

For this parameter set, MATLAB gives the corrected disease-free quantities

$$S_0 = 4000, Y_0 = 19.920223641423,$$
$$H_0 = 114.000798719370,$$
$$\Gamma_0 = 0.399909720116, \mathcal{R}_0 = 7.124438530772.$$

Hence,

$$E_0 = (4000,0,0,0,19.920223641423, 114.000798719370).$$

Here, Γ_0 is the total infectious removal coefficient evaluated at the disease-free resource levels. Since $\mathcal{R}_0 > 1$, the infected subsystem is expected to contain an unstable direction. This is confirmed by the eigenvalues

$$-0.0200,\quad -0.0200,\quad -1.2144,\quad 0.5445,\quad -0.1337,\quad -0.1873.$$

The positive eigenvalue 0.5445 establishes the local instability of E_0, in agreement with Theorem 2. The remaining eigenvalues have negative real parts and therefore correspond to decaying demographic and resource modes.

Table 2. Normalized forward sensitivity indices of $\mathcal{R}_0$ for the illustrative baseline parameter set

Parameter	Index	Parameter	Index	Parameter	Index
β	1.0000	Λ	1.0000	μ	−1.1241
κ	0.0741	d	−0.0750	γ_0	−0.2000
γ_1	−0.2495	γ_2	−0.4255	m	0.1499
n	0.0635	a	−0.1661	b	−0.6310
c	0.0000	Π	−0.5259	Π_H	−0.1264
ξ	0.1676	q_1	0.0000	q_2	0.3583
ξ_H	0.3362	θ	−0.2098	ω	0.0000

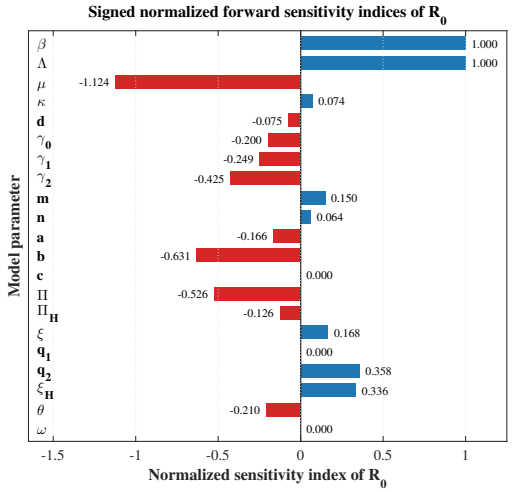

Signed indices from Table 2.

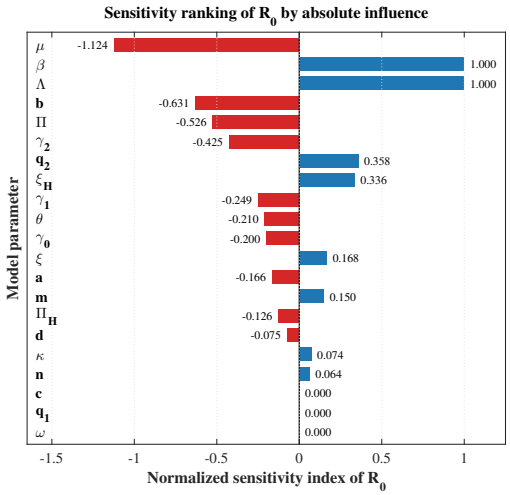

Parameters ordered by decreasing absolute sensitivity.

Figure 2. Sensitivity analysis of $\mathcal{R}_0$ at $Y_0 = 19.9202$, $H_0 = 114.0008$, and $\mathcal{R}_0 = 7.1244$. Positive bars increase the threshold under a relative parameter increase; negative bars decrease it.

Table 3. Illustrative baseline parameter values used in the numerical experiments

Parameter	Value	Interpretation	Source/status
Λ	80	recruitment into the susceptible population	synthetic benchmark
μ	0.02	natural removal rate	synthetic benchmark
β	0.0025	baseline transmission coefficient	synthetic benchmark
κ	0.25	progression rate from exposed to infectious	synthetic benchmark
d	0.03	disease-induced removal rate	synthetic benchmark
γ_0	0.08	baseline recovery contribution	synthetic benchmark
γ_1, γ_2	$0.25, 0.20$	resource-enhanced recovery effects	synthetic benchmark
m, n	$30, 20$	half-saturation constants in $\Gamma(Y, H)$	synthetic benchmark
a, b, c	$0.01, 0.015, 0.01$	incidence damping and saturation coefficients	synthetic benchmark
Π	5	socio-economic replenishment	synthetic benchmark
ξ	0.08	natural decay rate of Y	synthetic benchmark
q_1, q_2	$0.002, 0.0015$	infection-induced depletion and healthcare operating cost in Y	synthetic benchmark
Π_H	3	healthcare replenishment	synthetic benchmark
ξ_H	0.07	natural decay rate of H	synthetic benchmark
θ	0.25	reinforcement of healthcare capacity by socio-economic support	synthetic benchmark
ω	0.0015	infection-induced healthcare depletion	synthetic benchmark
ϱ	0.35	treatment-control efficiency	synthetic benchmark
σ_H	4	healthcare-reinforcement efficiency	synthetic benchmark
A_E, A_I	$20, 40$	state weights in the objective functional	modeling choice
B_1, B_2, B_3	$80, 60, 50$	quadratic control-cost weights	modeling choice

The scalar equilibrium equation $\Psi(I) = 0$ yields

$$E^* = (495.0035405633,\ 259.6293673657,\ 253.3934715387,\ 2611.8834132242,\ 8.2824569200,\ 11.2657732776).$$

Direct substitution into the six equilibrium equations gives the maximum absolute residual

$$\max_{1\le j\le 6} |f_j(E^*)| = 1.776 \times 10^{-14},$$

which confirms the numerical consistency of the computed equilibrium to machine precision. The eigenvalues of the full Jacobian at E^* are

$$-0.0200, \qquad -0.6123,$$
$$-0.0693 \pm 0.0827\,\mathrm{i}, \qquad -0.4953 \pm 0.0972\,\mathrm{i}.$$

All real parts are strictly negative. Therefore, the computed endemic equilibrium is locally asymptotically stable for the baseline parameter set. The two complex-conjugate pairs indicate damped oscillatory modes, whereas the two negative real eigenvalues describe nonoscillatory decay. This conclusion applies only to the displayed parameter set and is not asserted as a parameter-independent stability theorem.

Figure 3 displays the uncontrolled trajectories, the infectious trajectory relative to the disease-free and endemic reference levels, and the phase portrait in the (E, I)-plane.

The endemic resource levels are substantially below their disease-free values. In particular,

$$\frac{Y_0 - Y^*}{Y_0} \times 100\% = 58.42\%,$$
$$\frac{H_0 - H^*}{H_0} \times 100\% = 90.12\%.$$

Thus, persistent infection is accompanied by marked degradation of both support variables in the baseline regime. The reduction in Y is generated by the infection-pressure term $q_1 IY$ and the healthcare operating-cost term $q_2 HY$, whereas the reduction in H is driven by the depletion term ωIH.

Figures 4 and **5** present the converged control profiles and the controlled-versus-uncontrolled state trajectories.

The converged MATLAB solution gives

$$J_h = 10036.7976299844.$$

This value is the discretized weighted sum of epidemic burden and intervention effort for the specific weights in **Table 3**; it has no independent epidemiological unit and should only be compared with objective values obtained under the same weights, horizon, and discretization.

The controlled terminal state is

$$(S, E, I, R, Y, H)(120) = (3953.408738,\ 0.808589,\ 0.222440,\ 6.735835,\ 19.717276,\ 115.128841).$$

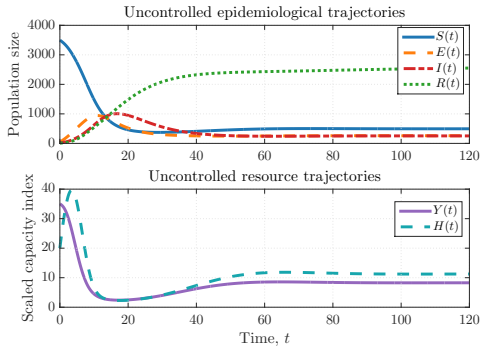

Uncontrolled epidemiological and resource trajectories on $[0, 120]$.

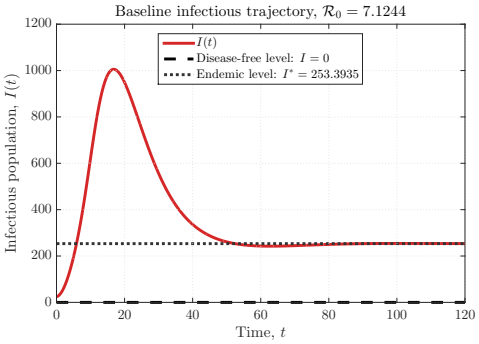

$I(t)$ relative to $I = 0$ and $I^* = 253.3935$.

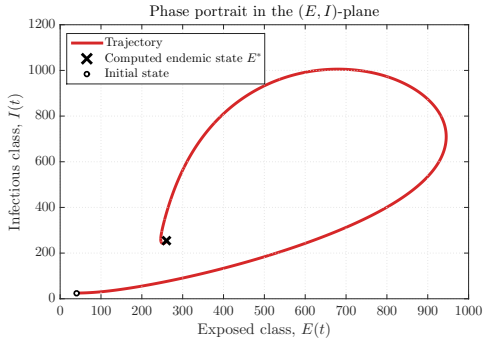

Trajectory in the (E, I)-plane and the computed endemic state.

Figure 3. Threshold and endemic diagnostics for the baseline parameter set. The value $\mathcal{R}_0 = 7.1244 > 1$ is consistent with instability of the disease-free equilibrium, while the spectrum of $J(E^*)$ establishes local stability of the computed endemic equilibrium.

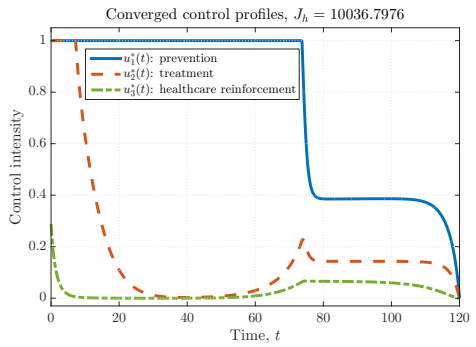

Converged profiles $u_1^*(t)$, $u_2^*(t)$, and $u_3^*(t)$.

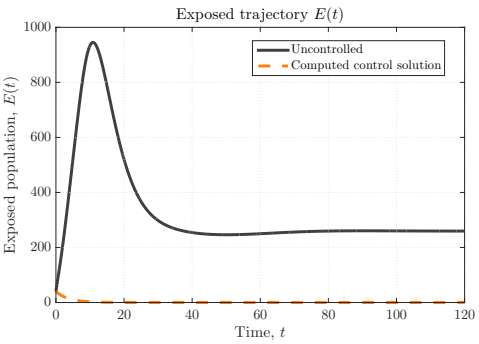

Controlled and uncontrolled exposed trajectories.

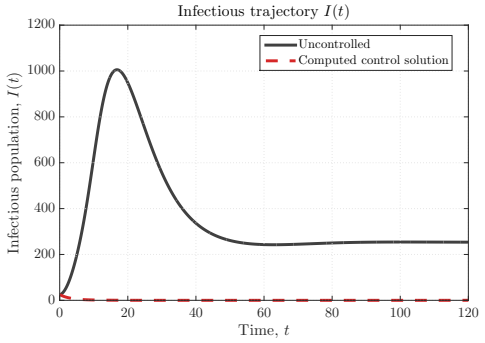

Controlled and uncontrolled infectious trajectories.

Figure 4. Computed controls and principal epidemiological effects on $[0, 120]$. Solid curves denote the uncontrolled solution and dashed curves denote the trajectory generated by the converged control profiles.

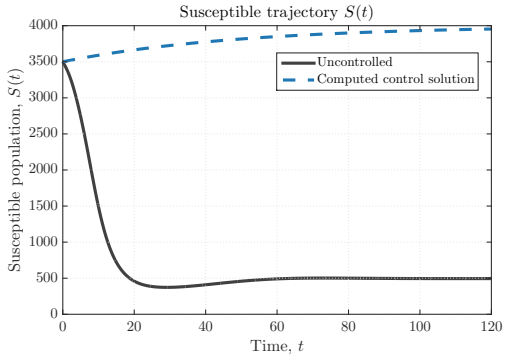

Susceptible trajectory $S(t)$.

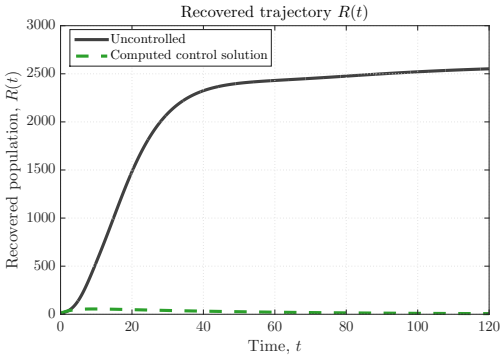

Recovered trajectory $R(t)$.

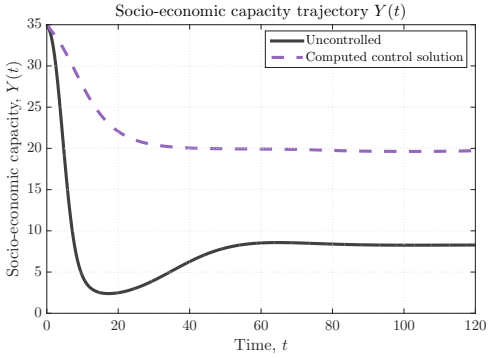

Socio-economic capacity $Y(t)$.

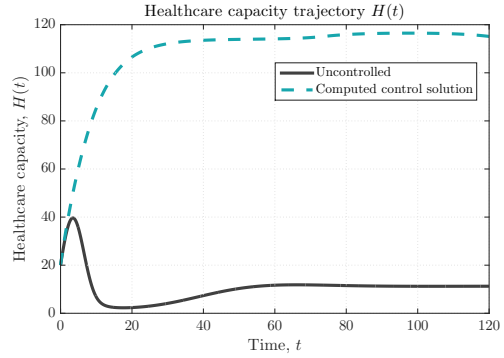

Healthcare capacity $H(t)$.

Figure 5. Additional controlled and uncontrolled state comparisons on $[0, 120]$. Solid curves denote the uncontrolled solution and dashed curves denote the controlled solution.

The uncontrolled peaks are

$$\max E(t) = 945.195697,$$
$$\max I(t) = 1005.562958,$$

whereas the controlled maxima are

$$\max E(t) = 40, \qquad \max I(t) = 25.$$

Thus, relative to the uncontrolled simulation, the computed controls reduce the exposed and infectious peaks by approximately 95.77% and 97.51%, respectively. Since the controlled maxima coincide with the initial values, the converged controls prevent any post-initial amplification of the exposed and infectious classes over the simulated horizon. At $t = 120$, both infected classes are close to zero, $Y(t)$ is close to its disease-free level, and $H(t)$ is slightly above H_0 because of the healthcare-reinforcement control. These statements characterize the computed solution of the Pontryagin necessary conditions and do not establish global numerical optimality.

6.2. Impact of economic and resource parameters

The resource-parameter sweeps use

$$\Pi \in \{2.5, 5, 7.5, 10\}, \qquad \Pi_H \in \{1.5, 3, 4.5, 6\},$$
$$\theta \in \{0.13, 0.25, 0.38, 0.50\},$$

and simultaneous scaling factors $0.5, 1, 1.5, 2$ for the pair (a, b), with all remaining parameters fixed at their baseline values.

Increasing Π raises the socio-economic support level, which both enlarges the incidence denominator $(1 + aY)$ and increases the recovery contribution $\gamma_1 Y/(m + Y)$. Over the tested range, the infectious peak decreases from approximately 1091.93 to 845.33, which corresponds to a reduction of 22.58%. Increasing Π_H acts analogously through $(1 + bH)$ and $\gamma_2 H/(n + H)$; the infectious peak decreases from approximately 1061.01 to 909.77, a reduction of 14.26%.

Increasing θ strengthens the transfer from socio-economic support to healthcare capacity. Under the baseline regime, this increases $H(t)$ and decreases the infectious peak from approximately 1035.52 to 952.24, an 8.04% reduction over the tested range. Simultaneously scaling (a, b) strengthens the direct resource-dependent damping of the force of infection; increasing the scaling factor from 0.5 to 2 reduces the infectious peak from approximately 1046.11 to 930.91, an 11.01% reduction.

6.3. Impact of intervention and efficiency parameters

The constant-control sweeps use

$$u_j \in \{0, 0.25, 0.50, 0.75\}, \qquad j = 1, 2, 3.$$

The prevention control u_1 acts directly on the force of infection through the factor $(1 - u_1)$, whereas the treatment control u_2 increases infectious removal through the additive term ϱu_2. Increasing u_1 from 0 to 0.75 reduces the infectious peak from approximately 1005.56 to 263.66, a reduction of 73.78%. Increasing u_2 over the same range reduces the infectious peak to approximately 386.17, a reduction of 61.60%.

The reinforcement control u_3 enters only the healthcare equation through $\sigma_H u_3$; its effect on infection is therefore indirect, operating through the transmission-damping and recovery-enhancement roles of H. Increasing u_3 from 0 to 0.75 reduces the infectious peak from approximately 1005.56 to 909.77, while increasing the terminal healthcare level from approximately 11.25 to 20.77.

The treatment-efficiency sweep uses

$$\varrho \in \{0.17, 0.35, 0.52, 0.70\}, \qquad u_2 = 0.5.$$

Increasing ϱ strengthens the conversion of treatment effort into infectious removal and reduces the infectious peak from approximately 692.92 to 305.03, a reduction of 55.98%. The healthcare-reinforcement sweep uses

$$\sigma_H \in \{2, 4, 6, 8\}, \qquad u_3 = 0.5.$$

Increasing σ_H raises the healthcare trajectory and reduces the infectious peak from approximately 971.52 to 881.76, a reduction of 9.24%. These simulations distinguish control intensity from control efficiency: u_2 and u_3 represent implementation levels, whereas ϱ and σ_H determine the corresponding conversion gains.

6.4. General synthesis

The MATLAB simulations support four model-specific conclusions. First, $\mathcal{R}_0 > 1$ and the positive eigenvalue of $J(E_0)$ are consistent with invasion from the disease-free state. Second, the computed endemic equilibrium satisfies the equilibrium equations to machine precision and is locally asymptotically stable for the baseline set, with damped oscillatory components in the local dynamics. Third, the converged control profiles suppress post-initial growth of the exposed and infectious classes and return the resource variables close to their disease-free levels. Fourth, socio-economic replenishment, healthcare replenishment, resource transfer, intervention intensity, and intervention efficiency act through mathematically distinct pathways and therefore produce quantitatively different effects on the epidemic trajectories. All interpretations are conditional on the synthetic parameter set, the selected time horizon, and the objective weights. (**Figures 6–9**)

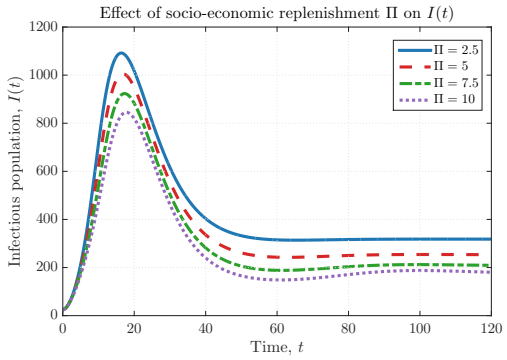

$I(t)$ for $\Pi = 2.5, 5, 7.5, 10$.

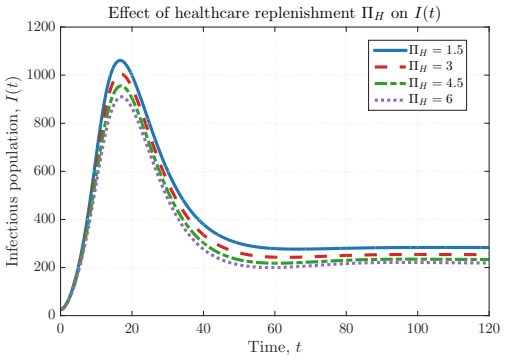

$I(t)$ for $\Pi_H = 1.5, 3, 4.5, 6$.

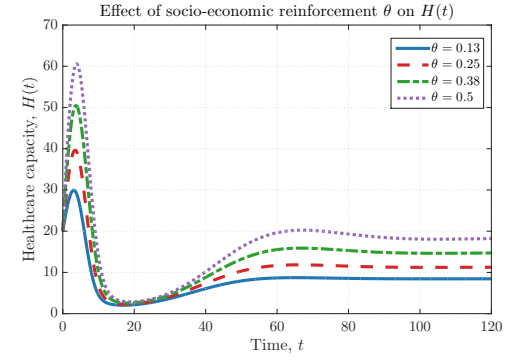

$H(t)$ for $\theta = 0.13, 0.25, 0.38, 0.50$.

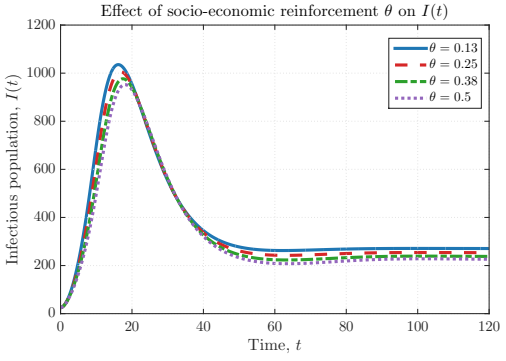

$I(t)$ for $\theta = 0.13, 0.25, 0.38, 0.50$.

Figure 6. Resource-inflow and transfer sweeps with all unvaried quantities fixed at their baseline values

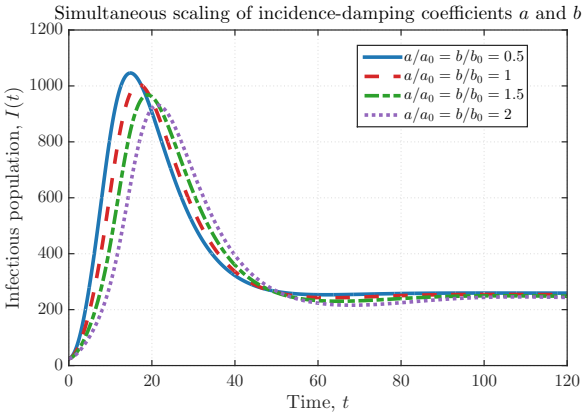

Figure 7. Infectious trajectories obtained by multiplying the incidence-damping pair (a, b) simultaneously by $0.5, 1, 1.5, 2$, with all remaining parameters fixed at their baseline values

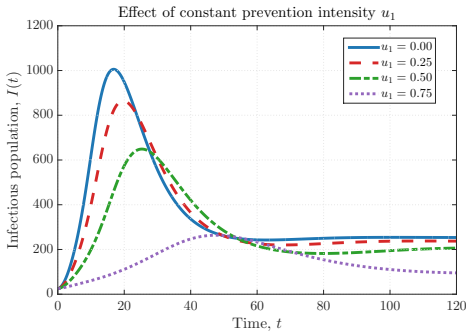

$I(t)$ for $u_1 = 0, 0.25, 0.50, 0.75$.

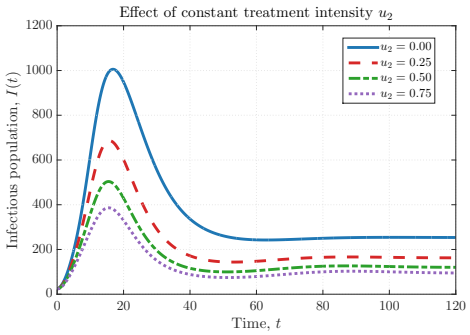

$I(t)$ for $u_2 = 0, 0.25, 0.50, 0.75$.

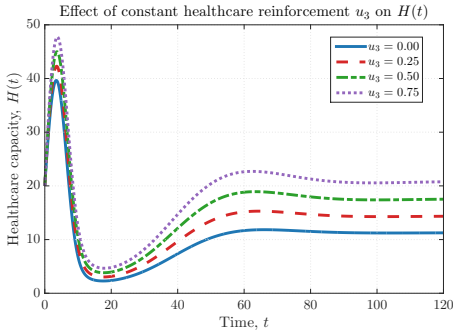

$H(t)$ for $u_3 = 0, 0.25, 0.50, 0.75$.

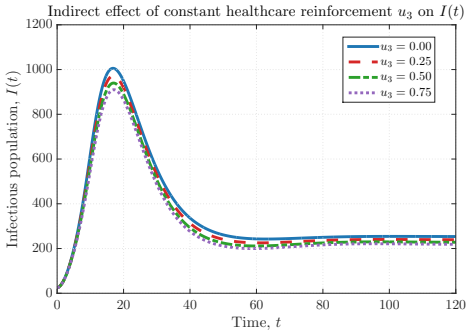

$I(t)$ for $u_3 = 0, 0.25, 0.50, 0.75$.

Figure 8. Constant-control sweeps showing the direct effects of prevention and treatment and the indirect epidemiological effect of healthcare reinforcement

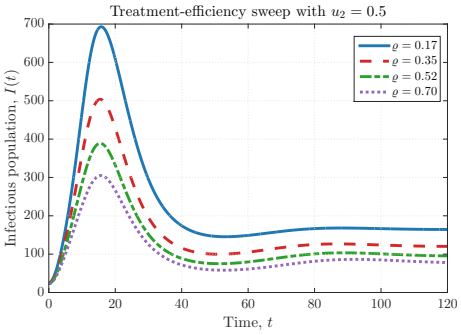

$I(t)$ for $\varrho = 0.17, 0.35, 0.52, 0.70$ with $u_2 = 0.5$.

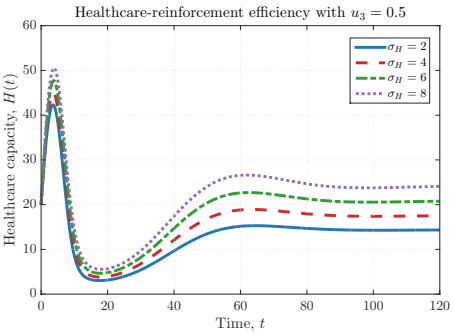

$H(t)$ for $\sigma_H = 2, 4, 6, 8$ with $u_3 = 0.5$.

Figure 9. Efficiency sweeps separating intervention intensity from treatment efficiency ϱ and healthcare-reinforcement efficiency σ_H

7. Conclusion

We analyzed a deterministic SEIR model coupled with scaled socio-economic and healthcare-capacity indices. The coupling is bidirectional: Y and H reduce incidence and enhance recovery, while infection and healthcare operation reduce the available capacities.

The nonnegative orthant is forward invariant, and comparison estimates yield bounded global solutions. The disease-free resource levels are determined by the coupled equations $\Pi - \xi Y_0 - q_2 H_0 Y_0 = 0$ and $\Pi_H - \xi_H H_0 + \theta Y_0 = 0$. Using these corrected levels, we derived $\mathcal{R}_0$ and proved local asymptotic stability of the disease-free equilibrium for $\mathcal{R}_0 < 1$ and instability for $\mathcal{R}_0 > 1$. For $\mathcal{R}_0 > 1$, the endemic-equilibrium equations reduce to a scalar equation that guarantees at least one positive root; Proposition 4 gives a sufficient monotonicity condition for uniqueness.

For the illustrative baseline set, $\mathcal{R}_0 = 7.1244$, the disease-free equilibrium has a positive eigenvalue, and the computed endemic equilibrium satisfies the steady-state equations with a residual below 1.776×10^{-14}. The six eigenvalues of the full endemic Jacobian have negative real parts, establishing local asymptotic stability of this specific equilibrium. No general endemic-stability claim is made outside this parameter set.

The optimal-control problem includes prevention, treatment, and healthcare reinforcement. The admissible set is treated as a closed, bounded, convex subset of $(L^2(0,T))^3$; existence of an optimal control follows by weak compactness and lower semicontinuity, and the Pontryagin principle yields the adjoint equations and projected control formulas. Under the selected weights, the converged solution of the necessary optimality system produces lower exposed and infectious trajectories than the uncontrolled simulation and preserves higher resource trajectories after the initial transient. The forward-backward sweep converged under the stated stopping criterion and produced the discrete objective value $J_h = 10036.7976$.

The normalized forward sensitivity analysis was recomputed from the coupled disease-free resource system. In the baseline set, β and Λ have unit positive indices, whereas μ, b, Π, and γ_2 provide the largest negative effects in magnitude. The signs of resource-mediated sensitivities are parameter-dependent and were therefore reported numerically rather than asserted universally.

The parameters are synthetic and are not calibrated to a particular epidemic. The results should therefore be interpreted as qualitative consequences of the model architecture, not as forecasts or direct policy estimates. Future work may incorporate data calibration, stochastic perturbations, reaction-diffusion effects, time delays, and spatial heterogeneity, following related stochastic and spatial epidemic frameworks.[27,28]

Acknowledgments

None.

Funding

None.

Conflict of interest

The authors declare no conflict of interest.

Author contributions

Conceptualization: Yassine Sabbar, Necati Özdemir
Formal analysis: All authors
Methodology: Necati Özdemir
Writing-original draft: Khaddouj Taifi, Yassine Sabbar
Writing-review & editing: Necati Özdemir

Availability of data

Not applicable.

AI tools statement

The authors used Grammarly and AI-based language enhancement tools solely for improving grammar, spelling, and overall language clarity during the preparation of this manuscript. These tools did not contribute to the study design, data analysis, results, or scientific conclusions.

References

1. Martcheva M. *An Introduction to Mathematical Epidemiology*. New York, NY: Springer; 2015. https://doi.org/10.1007/978-1-4899-7612-3
2. Brauer F, Castillo-Chavez C, Feng Z. *Mathematical Models in Epidemiology*. New York, NY: Springer; 2019. https://doi.org/10.1007/978-1-4939-9828-9
3. Espinosa O, Franco OH, Ospina M, Carabalí M, Baeza-Yates R. The value of mathematical modelling approaches in epidemiology for public health decision making. *Colomb J Anesthesiol*. 2024;52(1):e1079. https://doi.org/10.5554/22562087.e1079
4. Managi S, Chen Z. Social-economic impacts of epidemic diseases. *Technol Forecast Soc Change*. 2022;175:121316. https://doi.org/10.1016/j.techfore.2021.121316
5. Nyaruaba R, Okoye CO, Akan OD, et al. Socio-economic impacts of emerging infectious diseases

in Africa. *Infect Dis (Lond)*. 2022;54(5):315-324. https://doi.org/10.1080/23744235.2021.2022195

6. Feng Z, Liang X, Cai B. Impact of the epidemic on the world economy. *MATEC Web Conf*. 2022;355:02045. https://doi.org/10.1051/matecconf/202235502045
7. Abdelrahman HA, Hemstreet WG, Roy LA, Hanson TR, Beck BH, Kelly AM. Epidemiology and economic impact of disease-related losses on commercial catfish farms: A seven-year case study from Alabama, USA. *Aquaculture*. 2023;566:739206. https://doi.org/10.1016/j.aquaculture.2022.739206
8. Zaitseva NV, Popova AY, Kleyn SV, et al. Modifying impact of environmental factors on the course of an epidemic process. *Hyg Sanit*. 2022;101(11):1274-1282. https://doi.org/10.47470/0016-9900-2022-101-11-1274-1282
9. Gorbach PM, Ryan C, Saphonn V, Detels R. The impact of social, economic and political forces on emerging HIV epidemics. *AIDS*. 2002;16(Suppl 4):S35-S43. https://doi.org/10.1097/00002030-200216004-00006
10. Boucekkine R, Carvajal A, Chakraborty S, Goenka A. The economics of epidemics and contagious diseases: An introduction. *J Math Econ*. 2021;93:102498. https://doi.org/10.1016/j.jmateco.2021.102498
11. Ogunbameru A, Swayze S, Liu K, Mishra S, Sander B. Long-term healthcare resource use and cost associated with COVID-19 disease from a health system perspective. An equity-focused population-based cohort study. *medRxiv*. Preprint posted January 18, 2026. https://doi.org/10.64898/2026.01.16.26344255
12. Guo J, Yan B, Yang Y, Ning Y, Zhou Y, Zhang R, et al. Modeling healthcare resource dynamics and its application based on interregional population mobility. *Front Public Health*. 2025;13:1582024. https://doi.org/10.3389/fpubh.2025.1582024
13. Hall RJ. Modeling the effects of resource-driven immune defense on parasite transmission in heterogeneous host populations. *Integr Comp Biol*. 2019;59(5):1253-1263. https://doi.org/10.1093/icb/icz074
14. Afzal S, Maciejewski R, Ebert DS. Visual analytics decision support environment for epidemic modeling and response evaluation. In: *2011 IEEE Conference on Visual Analytics Science and Technology (VAST)*. IEEE; 2011:191-200. https://doi.org/10.1109/VAST.2011.6102457
15. Saha S, Samanta GP, Nieto JJ. Epidemic model of COVID-19 outbreak by inducing behavioural response in population. *Nonlinear Dyn*. 2020;102(1):455-487. https://doi.org/10.1007/s11071-020-05896-w
16. Yi N, Zhang Q, Mao K, Yang D, Li Q. Analysis and control of an SEIR epidemic system with nonlinear transmission rate. *Math Comput Model*. 2009;50(9-10):1498-1513. https://doi.org/10.1016/j.mcm.2009.07.014
17. Sethi SP, Staats PW. Optimal control of some simple deterministic epidemic models. *J Oper Res Soc*. 1978;29(2):129-136. https://doi.org/10.1057/jors.1978.27
18. Hamou AA, Rasul RRQ, Hammouch Z, Özdemir N. Analysis and dynamics of a mathematical model to predict unreported cases of COVID-19 epidemic in Morocco. *Comput Appl Math*. 2022;41:289. https://doi.org/10.1007/s40314-022-01990-4
19. Özdemir N, Ucar E, Avcı D. Dynamic analysis of a fractional SVIR system modeling an infectious disease. *Facta Univ Ser Math Inform*. 2022;37(3):605-619. https://doi.org/10.22190/FUMI211020042O
20. Bhatter S, Kumawat S, Bhatia B, Purohit SD. Analysis of COVID-19 epidemic with intervention impacts by a fractional operator. *Int J Optim Control Theor Appl*. 2024;14(3):261-275. https://doi.org/10.11121/ijocta.1515
21. Evirgen F, Özkose F, Yavuz M, Özdemir N. Real data-based optimal control strategies for assessing the impact of the Omicron variant on heart attacks. *AIMS Bioeng*. 2023;10(3):218-239. https://doi.org/10.3934/bioeng.2023015
22. Kaushik R. Mathematical epidemic model having two latent stages of exposed individuals. *Trans Comput Model Intell Syst*. 2026;3:10045. https://doi.org/10.65112/tcmis.10045
23. Diala LC, Toyin AR, Emmanuel A. Stability analysis of the disease-free equilibrium of tuberculosis transmission dynamics incorporating drug resistance and vaccination. *Trans Comput Model Intell Syst*. 2026;3:10030. https://doi.org/10.65112/tcmis.10030
24. Mohan Raja M, Vijayakumar V, Tsai C-W, Veluvolu KC. Optimal control strategies and continuous dependence for stochastic Hilfer fractional systems with delay: A Volterra-Fredholm integrodifferential approach. *Optim Control Appl Methods*. 2025;46(6):2708-2726. https://doi.org/10.1002/oca.70024
25. Mohan Raja M, Vijayakumar V, Veluvolu KC, Shukla A, Nisar KS. Existence and optimal control results for Caputo fractional delay Clark's subdifferential inclusions of order $r \in (1, 2)$ with sectorial operators. *Optim Control Appl Methods*. 2024;45(4):1832-1850. https://doi.org/10.1002/oca.3125
26. Mohan Raja M, Vijayakumar V. Optimal control results for Sobolev-type fractional mixed Volterra-Fredholm type integrodifferential equations of order $1 < r < 2$ with sectorial operators. *Optim Control Appl Methods*. 2022;43(5):1314-1327. https://doi.org/10.1002/oca.2892
27. Su T, Kao Y, Jiang D. Analysis of a generalized stochastic population diffusion epidemic model

perturbed by Black-Karasinski process. *Nonlinear Dyn.* 2026;114(2):121. https://doi.org/10.1007/s11071-025-11990-8

28. Su T, Kao Y, Jiang D. Dynamical behaviors of a stochastic SIR epidemic model with reaction-diffusion and spatially heterogeneous transmission rate. *Chaos Solitons Fractals.* 2025;195:116283. https://doi.org/10.1016/j.chaos.2025.116283

Khaddouj Taifi *received the Ph.D. degree in applied informatics from Sultan Moulay Slimane University (USMS), Beni Mellal, Morocco, in 2017. She is currently an Assistant Professor with the Department of Informatics, Faculty of Sciences and Technology (FST), Moulay Ismail University (UMI), Errachidia. Her research interests include artificial intelligence, biomedical engineering, and their interdisciplinary applications. Her work focuses on developing intelligent systems for healthcare, medical image analysis, and machine learning-driven decision support systems. She has contributed to various research projects and publications in these domains, aiming to bridge the gap between AI and biomedical sciences.*
https://orcid.org/0009-0001-0221-9714

Yassine Sabbar *received the Ph.D. degree from Sidi Mohamed Ben Abdellah University (USMBA), Fez, Morocco, in 2021. He is currently an Associate Professor with Moulay Ismail University, Morocco, and an Associate Researcher with the IDMS Team, Faculty of Sciences and Technology (FST), Errachidia. He has a strong publication record, with over 50 well-indexed research papers in prestigious journals and international conferences. Additionally, he has edited a scientific book. His research interests include mathematical modeling, biostatistics, and stochastic analysis, with a focus on applying advanced mathematical techniques to real-world problems in science and engineering. He serves on the editorial boards of three indexed journals, contributing to the dissemination of knowledge in his field.*
https://orcid.org/0000-0002-1127-4395

Necati Özdemir *is a Professor and Head of the Department of Mathematics at Balıkesir University, Turkiye. He received his B.Sc. from Marmara University in 1992, his M.Sc. from the University of Warwick, UK, in 1997, and his Ph.D. from the University of Exeter, UK, in 2000. His research interests include control theory, optimization, fractional calculus, mathematical modeling, numerical methods, biological modeling, financial mathematics, and renewable energy. He has published extensively, serves on international editorial boards, and is recognized among the top 3% of scientists in Turkiye.*
https://orcid.org/0000-0002-6339-1868

An International Journal of Optimization and Control: Theories & Applications (https://accscience.com/journal/ijocta)